AFGL-TR-80-0278
ENVIRONMENTAL RESEARCH PAPERS, NO. 714

LEVEL

Vacuum Ultraviolet Airglow
and Stellar Observations on the
MSMP/TEM-1 Rocket Flight

R. E. HUFFMAN
D. E. PAULSEN
J. C. LARRABEE
V. C. BAISLEY
F. J. LeBLANC
D. S. FRANKEL
M. E. GERSH

15 September 1980

AERONOMY DIVISION   PROJECT 2123
AIR FORCE GEOPHYSICS LABORATORY
HANSCOM AFB, MASSACHUSETTS 01731
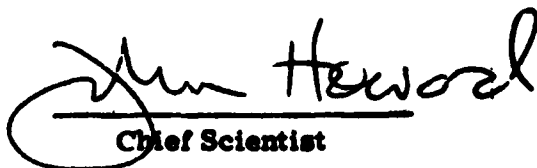
AIR FORCE SYSTEMS COMMAND, USAF

AD A099386

81 5 26 068

This report has been reviewed by the ESD Information Office (OI) and is releasable to the National Technical Information Service (NTIS).

This technical report has been reviewed and is approved for publication.

FOR THE COMMANDER

Chief Scientist

Qualified requestors may obtain additional copies from the Defense Technical Information Center. All others should apply to the National Technical Information Service.

SECURITY CLASSIFICATION OF THIS PAGE (When Data Entered)

REPORT DOCUMENTATION PAGE	READ INSTRUCTIONS BEFORE COMPLETING FORM

1. REPORT NUMBER	2. GOVT ACCESSION NO.	3. RECIPIENT'S CATALOG NUMBER
AFGL-TR-80-0278	AD-A099 386	

4. TITLE (and Subtitle)	5. TYPE OF REPORT & PERIOD COVERED
VACUUM ULTRAVIOLET AIRGLOW AND STELLAR OBSERVATIONS ON THE MSMP/TEM-1 ROCKET FLIGHT	Scientific. Interim
	6. PERFORMING ORG. REPORT NUMBER
	ERP No. 714

7. AUTHOR(s)	8. CONTRACT OR GRANT NUMBER(s)
R. E. Huffman V. C. Baisley M. E. Gersh* D. E. Paulsen F. J. LeBlanc J. C. Larrabee D. S. Frankel*	

9. PERFORMING ORGANIZATION NAME AND ADDRESS	10. PROGRAM ELEMENT, PROJECT, TASK AREA & WORK UNIT NUMBERS
Air Force Geophysics Laboratory (LKO) Hanscom AFB Massachusetts 01731	62324F 21230301

11. CONTROLLING OFFICE NAME AND ADDRESS	12. REPORT DATE
Air Force Geophysics Laboratory (LKO) Hanscom AFB Massachusetts 01731	15 Sep 80
	13. NUMBER OF PAGES
	60

14. MONITORING AGENCY NAME & ADDRESS(if different from Controlling Office)	15. SECURITY CLASS. (of this report)
	Unclassified
	15a. DECLASSIFICATION DOWNGRADING SCHEDULE

16. DISTRIBUTION STATEMENT (of this Report)

Approved for public release; distribution unlimited.

17. DISTRIBUTION STATEMENT (of the abstract entered in Block 20, if different from Report)

18. SUPPLEMENTARY NOTES

*Aerodyne Research, Inc., Bedford, MA

19. KEY WORDS (Continue on reverse side if necessary and identify by block number)

Vacuum ultraviolet
Airglow
Rocket flight

20. ABSTRACT (Continue on reverse side if necessary and identify by block number)

This report describes airglow and stellar observations made on the TEM-1 rocket flight as a part of the Multispectral Measurements Program (MSMP). The observations were in the 1100 to 3000 Å wavelength range from 65 to about 230-km altitude, and they include a number of scans of the viewing direction through the earth's horizon. Night airglow emissions observed include the hydrogen Lyman alpha geocorona and the oxygen Herzberg bands. A number of stars were observed including α-Eridanus, which is found to

DD FORM 1473 EDITION OF 1 NOV 65 IS OBSOLETE

20. Abstract (Continued)

match previous intensity measurements. The instrumentation consists of filter photometers with 10×10 element digicon spatial detectors and a spectrometer using a 1×36 element digicon for spectral resolution. The report describes the instrumentation, discusses the observations, and compares the results with previous measurements.

Preface

The authors gratefully acknowledge the support of the many people involved
with the rocket launch, with instrument design and fabrication, and with data reduc-
tion. Key personnel were R. Steeves and W. Miller, Aerospace Instrumentation
Division, AFGL; R. McInerney, Computation Branch, AFGL; D. Bedo, AFGL
(LKO); J. Bass and D. Schwank, Logicon; R. Moren, H. Tweed, F. Bonnano and
C. Sweeney, Northeastern University; J. Flemming, S. Russak and F. Steffens,
Martin Marietta; H. Alting-Mees and J. Choisser, Electron Vision Corp., and
L. Briggs and staff, Naval Ordnance and Missile Test Facility, White Sands
Missile Range. The encouragement and support of the MSMP manager,
A. McIntyre, Optical Physics Division, AFGL, is appreciated.

3

Contents

Illustrations

Tables

8

Vacuum Ultraviolet Airglow and Stellar
Observations on the MSMP/TEM-1 Rocket Flight

1. INTRODUCTION

This report describes observations made on the Multispectral Measurements
Program (MSMP) by the Air Force Geophysics Laboratory. It covers ultraviolet/
vacuum ultraviolet observations of airglow and stellar radiation made during the
TEM-1 (Target Engine Measurement) flight.

The ultraviolet region of the spectrum extends from about 4000 A (400 nm,
0.4 μm) near the blue end of the visible spectrum toward shorter wavelengths.
For measurements covered by this report, two general wavelength regions are
defined: the ultraviolet, from about 2000 to 3000 A; and the vacuum ultraviolet,
approximately about 1200 to 2000 A. Radiation with wavelengths shorter than about
2900 A cannot be transmitted either down or up through the atmosphere.

The use of ultraviolet radiation for military applications in space is made
attractive by the relatively low backgrounds encountered when observing the earth
or the earth's atmospheric limb. The recent AFGL satellite experiment, Vacuum
Ultraviolet Backgrounds,[1,2] helps to define this atmospheric radiation background.
The measurements discussed herein further characterize this radiative environ-
ment and tend to support both previous and later satellite observations.

The initial flight of the MSMP on 19 November 1977 occurred under night conditions at 2100 Mountain Standard Time (MST). A number of observations were made of the night airglow and of stars. These observations represent the first use of sensors based on digicon spatial imaging detectors on sounding rockets.[3] The present report demonstrates this new sensor technology through actual flight measurements. These digicon sensors consist of a 10 by 10 element array tube for use in photometers with rather broad wavelength bands isolated with filters and a 1 by 36 element tube used in a spectrograph, in order to obtain improved wavelength resolution. These tubes have been made with the "solar-blind" cathodes cesium iodide and cesium telluride; they represent a significant improvement in terms of size, weight, dynamic range, and photometric accuracy over spatial sensors available prior to this program.

Several airglow emission features in the night sky were observed. The hydrogen Lyman alpha geocorona at 1216 Å was readily observed. This radiation is the result of solar radiation multiply scattered by the small amount of atomic hydrogen in the earth's atmosphere. Azimuthal and elevation variation of this radiation was followed. The Herzberg bands of molecular oxygen are another well-known feature of the night airglow in the 2500 to 4000 Å region. In the present data, radiance profiles from movements of the line of sight through a range of elevation angles clearly show this emission. Emission also may have been seen from the Lyman-Birge-Hopfield (LBH) bands of nitrogen during scans through the atmospheric limb. It is not possible to state definitely that this limb emission is due to the LBH bands, as discussed herein. In fact, this source can be seriously considered only because LBH bands have recently been identified as a more or less constant feature of the night airglow as observed by the VUV Backgrounds experiment.[4,5]

The observation of VUV/UV stars and the earth limb.with the digicon detectors illustrates the use of these sensors for obtaining spatially resolved intensity measurements. The observed stars are useful in establishing the pointing direction, and their intensities are in good agreement with previous space measurements.

---

3. Russak, S. L., Flemming, J. C., Huffman, R. E., Paulsen, D. E., and Larabee, J. C. (1979) Development of Proximity and Electrostatically Focused Digicons for UV Measurements from Sounding Rockets, Air Force Geophysics Laboratory, Technical Report, AFGL-TR-79-0006.

4. Huffman, R. E., LeBlanc, F.J., Larrabee, J. C., and Paulsen, D. E. (1979) Satellite ultraviolet airglow backgrounds, Trans. American Geophysical Union, 60:901.

5. Huffman, R. E., LeBlanc, F.J., Larrabee, J. C., and Paulsen, D. E. (1980) Satellite vacuum ultraviolet airglow and auroral observations, J. Geophys. Res. 85:2201-2215.

2. INSTRUMENTATION

2.1 General

This report describes the data obtained from flight instrumentation using the digicon detector. This instrumentation was designed and fabricated by Martin-Marietta, Denver, Colorado, to specifications developed for the MSMP flights at AFGL. The instrument response was telemetered to ground receiving stations. The UV sensors on the payload also included two electrographic cameras provided by the Naval Research Laboratory (NRL). These instruments and results are not described in this report, although available from NRL. Observations by the cameras have been limited owing to the unplanned rapid motion of the line of sight.[6]

The goal of the ultraviolet instrumentation described herein was to obtain spatial and spectral data in the 1200 to 3000 Å wavelength region. An improvement in ultraviolet imaging techniques was desired; however, many possibilities were eliminated due to the relatively short observing time and to the need for maximum sensitivity over the total field at all times. The development and flight test of ultraviolet digicon imaging sensors on this program is one of its significant accomplishments. These tubes were made by the Electron Vision Division of SAI under a subcontract to Martin-Marietta.

2.2 TEM-1 Flight Sensors

The flight sensors on the TEM-1 rocket launch are described in Table 1. These instruments use digicon detectors, imaging devices of high sensitivity operating in the photon counting regime. High sensitivity and medium sensitivity spatial photometers were developed using 10 by 10 element digicon detectors. The frame rate was 0.1 second. After five frames of data observations with a given filter, a time period equal to one frame was used in moving the filter wheel to the next position. With four filters on each photometer, a total of 2.4 sec was required to complete the cycle. All 100 elements of the digicons were read out at the conclusion of each 0.1-sec frame and telemetered to the ground. The effect is equivalent to 100 independent photon-counting photometers, each covering a 0.4 by 0.4 degree square field and each capable of sensitivities approaching the noise limit of less than one count per second. The filters planned for HSP-51 were not utilized due to undependable filter wheel operation, and filter 1 was in place at all times. Due to the loss of sensor module attitude control, there was a more or

---

6. Opal, C., and Carruthers, G. (1979) Naval Research Laboratory, Personal communication.

Table 1. UV/VUV Flight Sensors for the TEM-1 Rocket Launch

Name and Serial Number	Cathode/ Window	Filter Number	Filter Type	Approx. Wavelengths Å
Medium Sensitivity Photometer				
MSP-11	CsI/MgF_2	1	MgF_2	1200-1800
		2	CaF_2	1250-1800
		3	Interference	1216
		4	Interference	1550
MSP-32	$CsTe/Al_2O_3$	1	Interference	2100
		2	Interference	2350
		3	Interference	2600
		4	Interference	2800
High Sensitivity Photometer				
HSP-51	CsI/MgF_2	1	Al_2O_3	1450-1800
UV Spectrometer				
SP-41	$CsTe/MgF_2$	---	---	1200-3000

less random set of filter position/pointing direction combinations. This limits the limb detail available with a given filter.

The UV spectrograph was developed with a 1 by 36 element digicon tube. The wavelength resolution although somewhat variable over the range was approximately 50 Å. The frame time was 0.1 sec, as for the photometers. A complete spectrum was obtained every 0.1 sec, so there is complete temporal coverage of the background radiation from this sensor. The field of view was about 1.5° square. The individual semiconductor diodes were larger for the 1 by 36 element tube, resulting in a larger dark count than for the 10 by 10 array tube.

The combination of photocathode surface, digicon window, and filter determines the wavelength response for the photometers. The filter can be a window material that has a transmission limit excluding light from shorter wavelengths. In this case, MgF_2 (1200 Å), CaF_2 (1250 Å), and sapphire, or Al_2O_3, (1450 Å) were all employed. It is also possible to use interference filters which have a bandwidth of about 150 to 200 Å. In some of these bands, the atmospheric radiative background is observed. This radiation and its variation with the various unplanned pointing directions during the flight constitute the primary results given by this report.

2.3 Photometers

A cross-section drawing of the photometer design, which applies to both the high and medium sensitivity photometer, is shown in Figure 1. It is based on a folded prime focus system. A plane folding mirror receives incoming radiation and reflects it to a parabolic mirror which focuses the field on the digicon window; the digicon is placed in a hole in the plane mirror; the four-position filter wheel is placed immediately in front of the digicon face. In order to preserve the focus, a filter or window is always installed in each of the four positions.
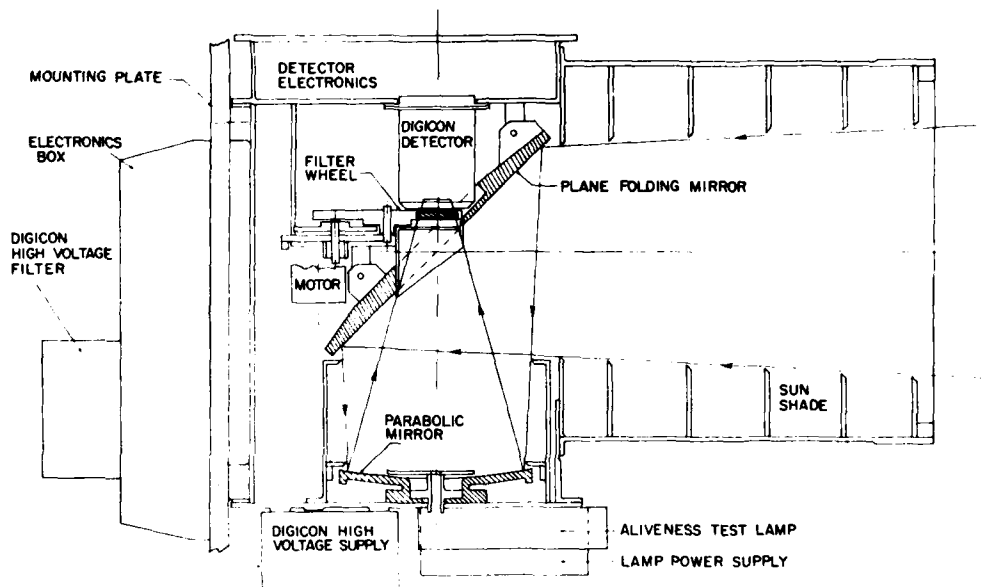
Figure 1. Cross-sectional View of Medium and High Sensitivity Photometers

The total field of view of both photometer types is approximately 4 by 4 degrees square, which results in individual element fields of view of about 0.4 by 0.4 degrees square for the 10 by 10 array. There is some deviation from these values at the edge of the field, as mapped during calibration and discussed in more detail in Section 3.

The medium sensitivity instrument has a 12-cm diameter, f/1.6 parabolic mirror with an effective aperture of about 84 cm^2, after allowance for the opening needed by the digicon.

13

For the high sensitivity unit, the corresponding dimensions are 21-cm mirror diameter with f/0.9 aperture ratio and an effective collecting aperture of 249 cm^2. All optical surfaces are aluminum, with a magnesium fluoride overcoating, in order to retain high reflectance at the shorter wavelengths.

A test lamp to establish instrument response to ultraviolet radiation and to indicate in a qualitative manner the relative response of the detector is used both on the ground and in flight. It is a small gas discharge tube containing xenon gas with or without an added trace amount of mercury vapor. The xenon emits primarily at the 1470 Å resonance line, and it is therefore suitable for the tubes with the CsI photocathode. For the tubes with a CsTe cathode, test lamps with added mercury are used, since they emit a relatively strong Hg line at 2537 Å. For ground tests at wavelengths shorter than about 2000 Å, where atmospheric oxygen absorbs, the oxygen is flushed from the body of the photometer with a stream of dry nitrogen gas. This procedure is essential if the photocathode is CsI. It is not absolutely necessary for digicons utilizing CsTe photocathodes, although frequently used, as it removes water vapor and gives a known gaseous environment. In order to keep the interiors of the sensors as clean and water-vapor free as possible, a purge flow of dry nitrogen is maintained at all times up to launch while the sensors are installed in the sensor module of the Aries rocket payload.

The 10 by 10 array proximity-focused digicon used for either type of photometer is shown in cross section in Figure 2. Electrons emitted due to photon absorption in the semitransparent photocathode are accelerated by approximately 25 kV applied between the photocathode and the diode array. The total flight distance is about 2 cm; this is short enough relative to the array element size to preserve the spatial properties of the observed optical field focused on the digicon window. The
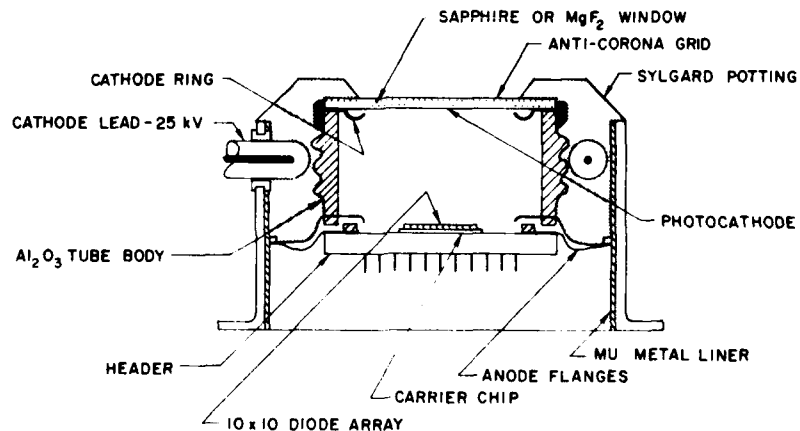
Figure 2. Cross-sectional View of Proximity Focused Digicon Tube

14

array consists of semiconductor diodes deposited on a single piece of silicon. These diodes are square with the length of each side being 0.107 cm. They are arranged in a square 10 by 10 array with the diodes spaced 0.127 cm between centers along each row or column. Narrow metallic connectors located between the diodes bring the signal counts of each pixel to the edge of the array for connection to the counting circuits. This array is mechanically bonded to an alumina header which also provides electrical connection between the array diode elements and the counting electronics. The diodes are biased at about 7 V. The detector tubes are sealed under high vacuum and potted to preclude high voltage problems.

The digicon and electronics circuitry are shown schematically in Figure 3. Each electron accelerated by the 25-kV field creates a charge pulse of about 6000 electrons when deposited in a semiconductor diode in the array. This rather small pulse of 6000 electrons must then be counted and ultimately telemetered to the ground-receiving station. There is a separate charge amplifier, filter-discriminator, and counter-shift register for each diode in the array. The sensor is therefore operating in the so-called staring mode with full coverage of the field at all times except for about 5 μsec of the 0.1-sec frame used to shift out the accumulated count.
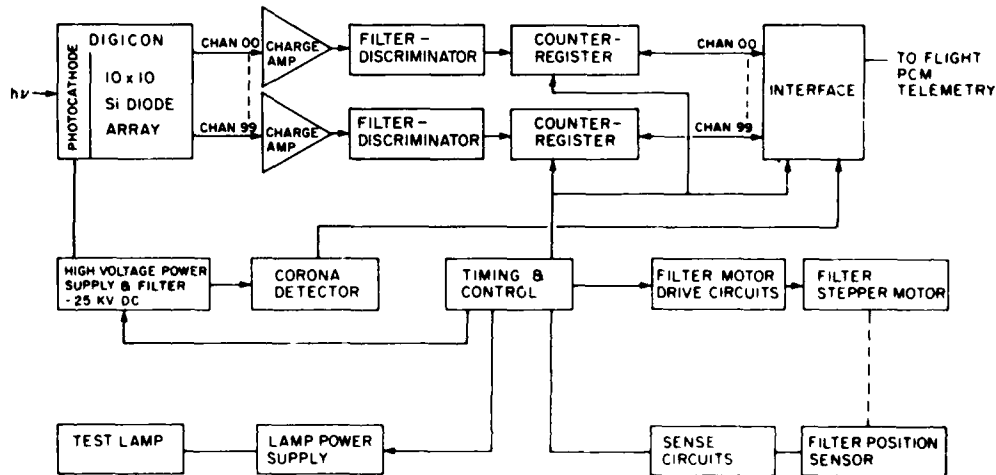
Figure 3. Schematic Diagram of Digicon Electronics Circuitry

In all digicons produced so far, some of the elements have not been usable either because they demonstrated no response, or because they had an excessive dark count. Two types of response with no external illumination should be mentioned. The signal channel noise is measured after the tube and counting electronics

15

are turned on, but before the 25-kV high voltage is on. Most noisy elements usually are observable at this point. The dark count is obtained after the high voltage is turned on. Counts are then seen on most channels. However, in the most favorable circumstances, the dark count on some elements of the 10 by 10 arrays can be as low as 0.03 count per second. An effort was made to keep the number of unusable elements in the center of the field to a minimum.

2.4 Spectrograph

The UV spectrograph using a digicon spatial detector is shown in Figure 4. Collimated light for the plane diffraction grating is produced by a set of metal grids. Thus, no entrance slit or collimating optics was utilized. The collimator consists of twenty-one grids with a pattern of 0.262-cm square openings electro-formed in stainless steel plates. The grid are spaced in a harmonic progression between the sunshade and the grating. In this manner, a square field of 1.5 degrees full width at half maximum is obtained. The unobscured aperture for the instrument is about 33 cm^2, after accounting for the collimating grids and the digicon obscuration.
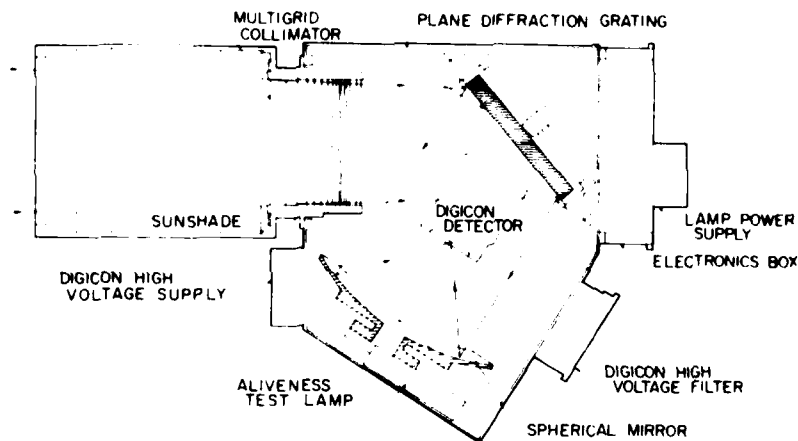
Figure 4. Cross-sectional View of UV Spectrograph

The dispersed radiation from the grating is focused by a spherical Schmidt-type imaging mirror onto the face of the digicon. This mirror has a focal length of 13.3 cm and is f/0.9. A test lamp similar to those in the photometers was used.

The 1 by 36 array digicon is considerably different from the 10 by 10 tubes described previously. A cross-section drawing is shown in Figure 5. The optical image on the face of the tube is focused on the array electrostatically. The outer

MgF FILTER FOR SHORT WAVELENGTHS

MgF WINDOW

CATHODE LEAD -25 kV

Al₂O₃ TUBE BODY

MU METAL SHIELD

ANODE FLANGE

QUARTZ ORDER SORTING FILTER FOR HIGH WAVELENGTHS

SYLGARD POTTING

CATHODE FLANGE

CsTe PHOTOCATHODE

ELECTRON OPTICS

HEADER

CARRIER CHIP

36 DIODE ARRAY
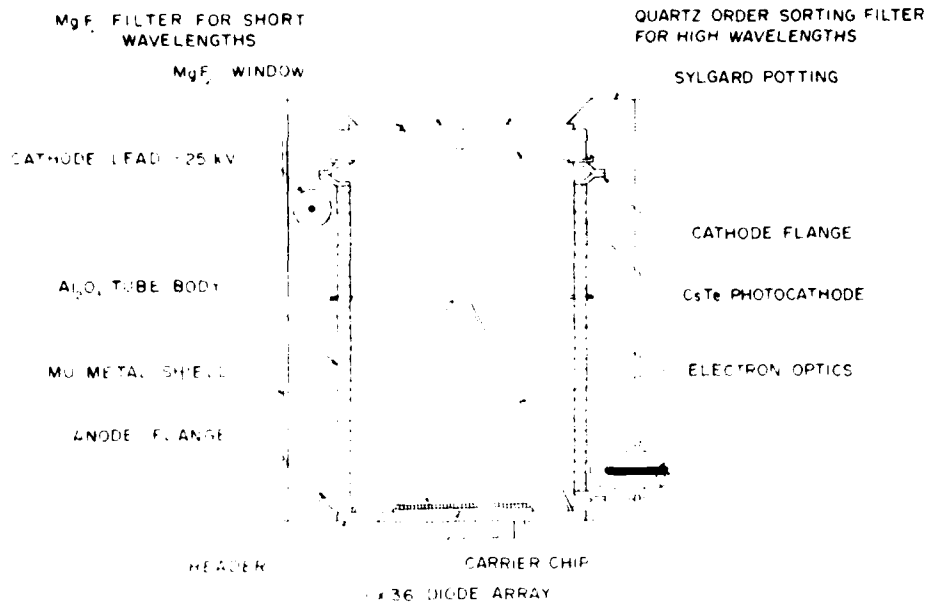
Figure 6. Cross-sectional View of Electrostatically Focused Digicon Tube

face of the tube is flat, whereas the inner face containing the photocathode is curved to match the Petzval curvature of the spectrometer field. The face of the tube contains a quartz filter to eliminate higher order images in the 2000 to 3000 A range and a MgF₂ filter on the short wavelength end to match the optical path. The diodes are 0.17 cm high and 0.057 cm wide, except for the three elements closest to the hydrogen Lyman alpha line. These are one half the width of the other elements. The field of view of each detector element is about 1.0" in height and 0.1 or 0.2" in width. From the photocathode to the array, there is a 1:2.5 de-magnification.

For data read out, the 1 × 36 array tube operates in a manner identical to the 10 by 10 tube with, however, only 36 channels of counting electronics in Figure 3. There are generally some channels either giving no response, or an excessively high count with no signal. A larger dark count is reasonable for this tube, as the size of the diode is larger. The most favorable dark count might be predicted to be about 10 counts per second, but in practice the best values are in the range 400 counts per second. Nevertheless, useful measurements have been obtained from the instrument. The development of the digicon tube into a dependable and available item is continuing, and it is anticipated that improved tubes will be available for future flights.

17

3. CALIBRATION AND TEST

3.1 Ultraviolet Calibration Facility

The flight instruments were given a number of calibrations against standard detectors. These measurements were largely accomplished in the vacuum chamber shown in Figure 6. The flight sensor being calibrated is placed on the gimbal mount table at the left part of the figure. It is then irradiated with collimated UV light of known flux (photon/sec cm^2). The counts observed compared to photons entering the instrument gives the sensitivity, which is then used to measure irradiance at the sensor in flight.

The gimbal mount can be moved over an angular range of ± 45 degrees in azimuth and in elevation. By this movement, the collimated beam is brought to focus by the photometer on each element of an array in turn. The motion is controlled by an HP-9810 programmable desk top calculator so that a standard pattern of 10×10 or 12×12 steps can be automatically scanned. The total field can be mapped in about 4-1/2 minutes. Every 0.1 sec the entire one hundred element frame is read out. The foregoing description refers to the 10×10 array photometers. A similar technique is used for the spectrometer.

Two general types of sources are available. Small gas discharge tubes provide a point-like source largely confined to one or a few emission lines. Discharge tubes emitting hydrogen Lyman alpha (1216 A), a xenon resonance line (1470 A), and a mercury resonance line (2537 A) were used. Interference filters helped to further isolate the lines. These sources provide a near uniform beam of about 35 cm dia at the test position, which approximates the diameter of the collimating mirror.

For more detailed wavelength coverage, a vacuum monochromator is used, as shown in the figure. A gas discharge source using helium with a trace of CO_2 provides a dense output of carbon monoxide fourth-positive bands throughout most of the region of interest here. The exit slit is replaced by an exit hole at the focus of the collimating mirror. The astigmatism of the monochromator leads to a collimated beam pattern that approximates a 3 mm high band across the field. With the monochromator, detailed wavelength response curves of the various filter-digicon combinations are obtainable.

The flux in the collimated beam is measured by the beam probe, a calibrated EMR 542F photomultiplier capable of being moved horizontally and vertically through the beam. The photocathode is CsTe. This tube is periodically calibrated against a standard photodiode supplied by National Bureau of Standards (NBS). This photodiode is rechecked at NBS approximately every year, and it is checked against other photocells at AFGL periodically. For many of these tests and for the dynamic range measurements reported later, a set of neutral density filters are used and calibrated at wavelengths of interest over a density range from about 0 to 6. A

18
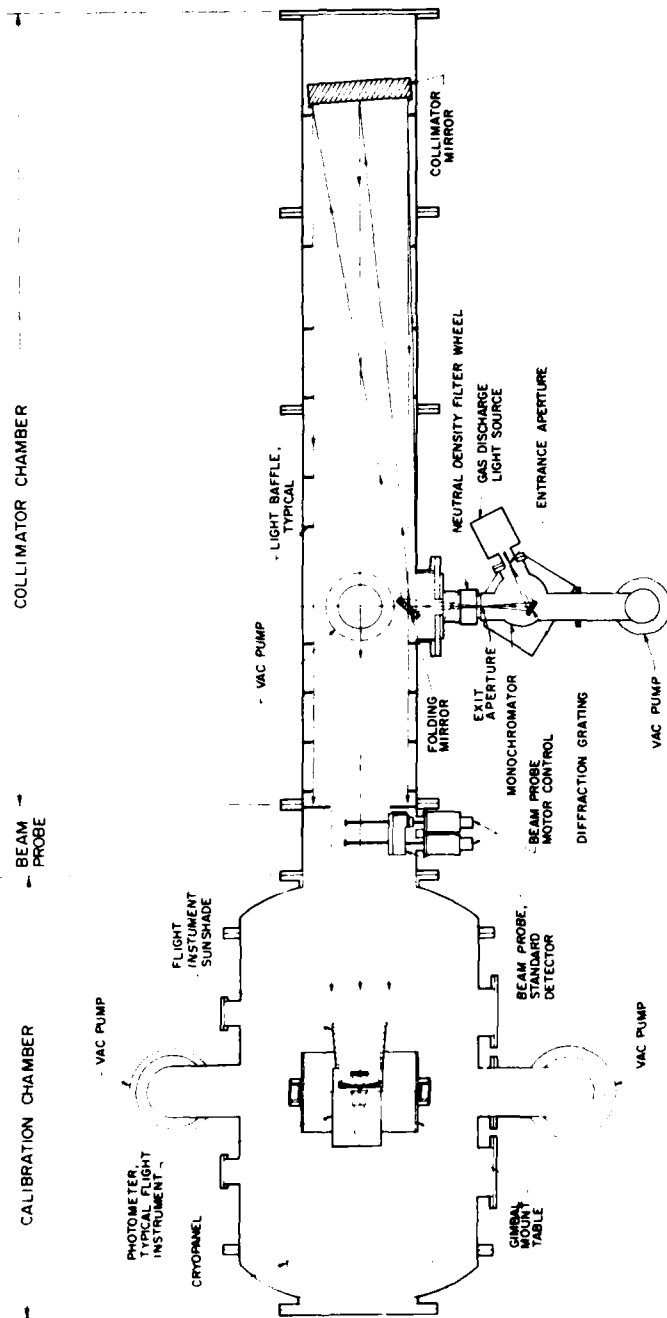
Figure 6. Ultraviolet Calibration Facility

19

discussion of the accuracy of the calibration has been made for a similar calibration and estimated to be within 15 percent in the most favorable circumstances.[1] The TEM-1 calibrations should be of equivalent accuracy.

3.2 Array Element Response

The response of a row of elements in a 10 × 10 array digicon to a spot of UV radiation scanned across the field is shown in Figure 7. The peak response is reasonably constant and the half-width in the central part of the row corresponds to approximately 0.4°, as planned. There are no dead or noisy diode elements in this particular row. In the data analysis, separate relative calibration factors are used to account for the sensitivity differences seen on individual elements. In Figure 7, the individual array elements are referred to as pixels, a contraction of picture elements. These calibrations were made on MSP-33, which is a part of the TEM-2 payload, but the observed response is very similar for the TEM-1 instrument. Similar observations were also made on the element-to-element response of the spectrograph.
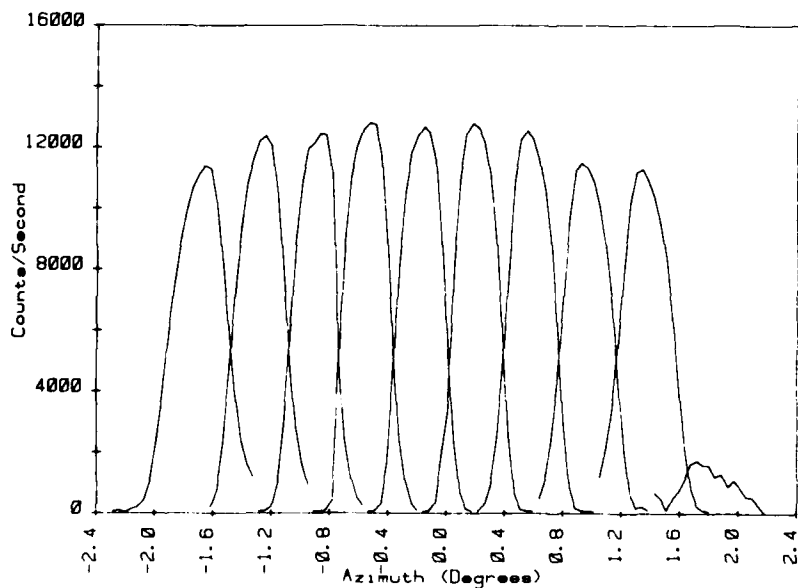
Figure 7. Response of a Row of Elements in 10 × 10 Digicon Array to a Spot of UV Radiation Scanned Across the Field

The angular extent of the total field for the 10 × 10 digicon is shown in Figure 8. As in the case of Figure 7, the digicon was in a photometer, so variations from design values may be due in part to the optical elements in the photometer. There is distortion at the corners and along the edges of the field with the total extent of the observed FOV closer to ±2.4° rather than the design value of ±2.0°. The inner pixels are close to the planned values. The degrees of azimuth and elevation shown are from the gimbal mount. Tests of more recently built photometers show improved field maps.
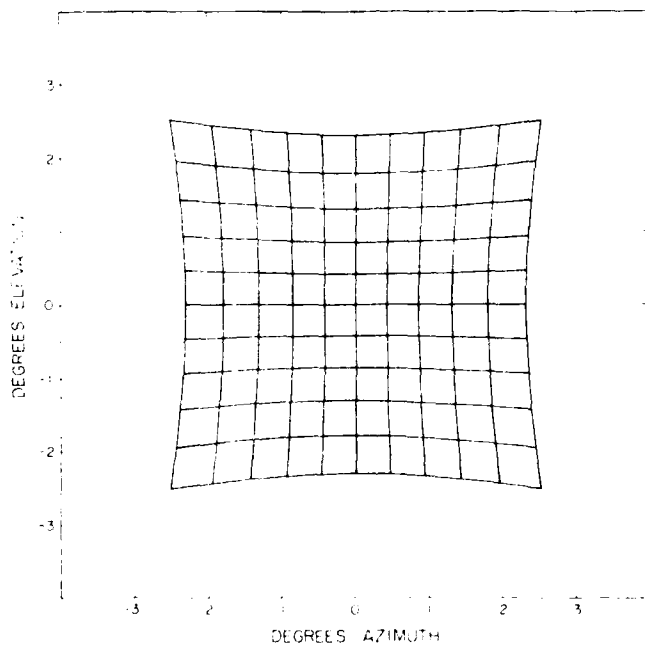
Figure 8. Angular Map of Total Field for a 10 × 10
Digicon Array Mounted in a Photometer

3.3 Out-of-field Response

The response to incident radiation arriving at the sensor at angles outside the geometric field of view (FOV) is obtained by motion of the gimbal mount in azimuth and elevation. In this way, the actual field of view, defined as the angular range between the points where the count rate drops to one-half of the value at the center of the field, can be obtained rather than a planned or design value. Any sort of light baffle problem or unrecognized scattering surface in the sensor will be found in this manner.

The observations are continued well beyond the design FOV to test further the baffles and to set limits on the effects of high intensity sources outside the FOV on the observed signal. The primary concern is an unplanned line of sight near the sun. Knowledge of this off-axis rejection is also useful in planning observations so that they are not unnecessarily restricted by solar radiation.

Figures 9 and 10 illustrate the off-axis rejection for HSP-52 and MSP-33, which are identical to the TEM-1 instruments in optical design. Note that the illustrative data shown includes both center and edge pixels. Other pixels at similar places in the field give similar responses. There are some edge effects seen in MSP-33, but they are not considered excessive. These response curves were obtained using the appropriate resonance lamps.
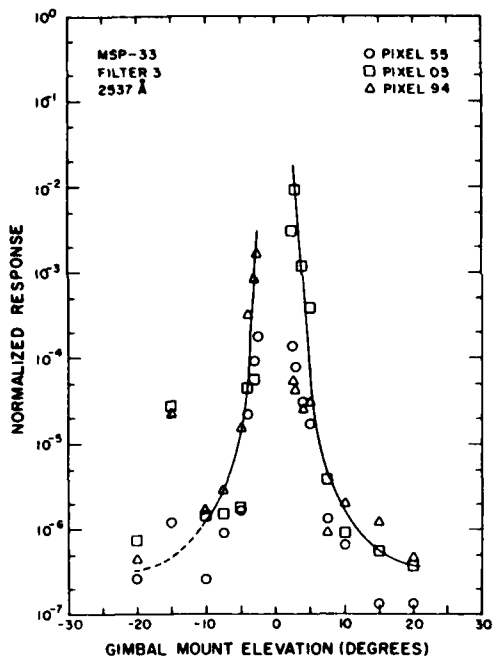
Figure 9. Off Axis Rejection Curves for UV Photometers Similar to the Medium Sensitivity Photometers on Board the MSMP TEM-1 Flight
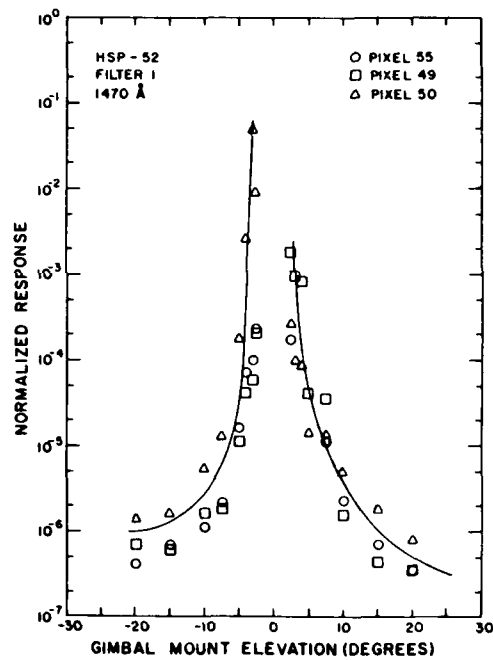
Figure 10. Off Axis Rejection Curves for UV Photometers Similar to the High Sensitivity Photometer on Board the MSMP TEM-1 Flight

The off-axis rejection of the spectrograph is not as complete as for the photometers. In addition, measurements are not available for the complete instrument, but only for the collimation grid assembly. However, it is likely that contributions

22

to the off-axis response from other elements of the spectrograph would be negligible compared to the grid assembly. The curves shown in Figure 11 were obtained by Martin Marietta Corporation before assembly, using visible light. The rejection is fairly good for one direction although not for the other, where there is considerable variation at somewhat regular intervals.
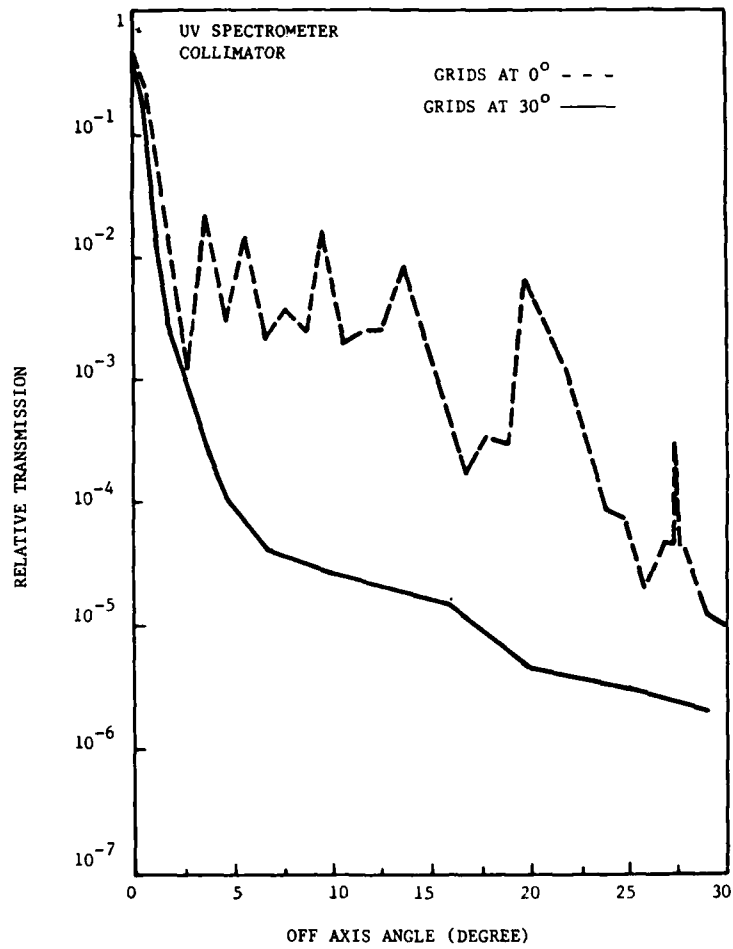
Figure 11. Off Axis Rejection of the UV Spectrometer Square Grid Collimator

3.4 Wavelength Coverage

The sensitivities of the filters used in the TEM-1 flight were determined in the calibration facility. In this report, relative sensitivities of the filters for each instrument are shown. The different curves can be correlated with filter positions by means of Table 1.

The observed relative sensitivity for MSP-11 is shown in Figure 12. The total range is determined by the CsI photocathode at the longer wavelength end and by windows for the upper two curves at the short wavelength cutoff. The two lower curves are obtained with interference filters. These VUV filters are not of the quality available in the UV. Their lower sensitivity however does have the effect of broadening the total dynamic range of the sensor so that larger irradiance values can be measured before the digicon is saturated.
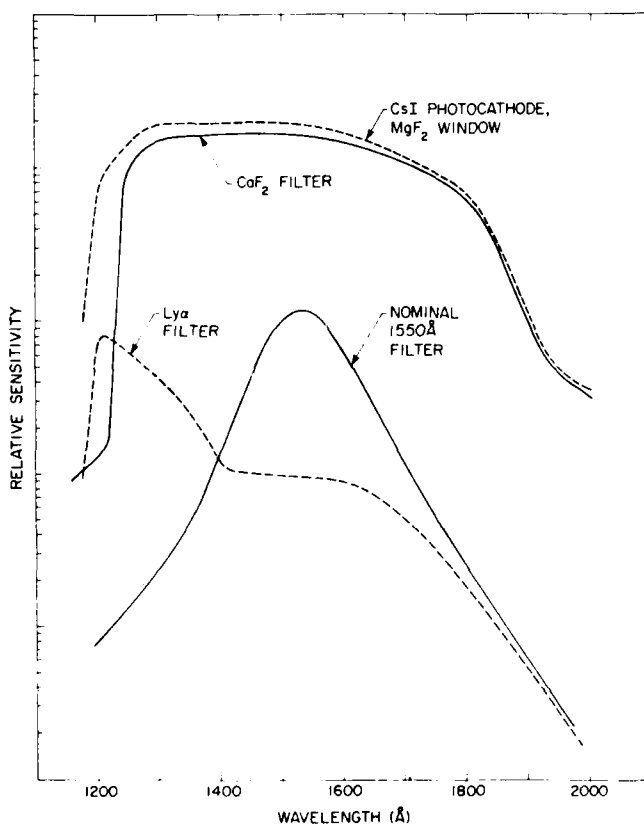
Figure 12. Measured Filter Relative Sensitivities for MSP-11

24

Figure 13 gives the relative sensitivites of the filters in MSP-32. They provide coverage of the range from about 1900 to 3000 Å. Although not shown in the figure, the CsTe quantum efficiency curve drops off sharply to longer wavelengths beyond about 3000 Å.

The planned filter sensitivities for the high sensitivity photometer are shown in Figure 14. The use of high-quality sapphire (Al_2O_3) either as a digicon window or as a filter results in a lower wavelength transmission limit of about 1450 Å. This limit prevents observation of several atmospheric lines such as hydrogen Lyman alpha (1216) and the oxygen lines at 1304 and 1356 Å. The quartz filter response beginning about 1600 Å can be used to isolate a band centered near 1500 Å by taking the difference in observed signal between the sapphire and quartz windows. While this can also be done using interference filters, there would be a loss of relative sensitivity. As mentioned earlier, problems with reliable operation of the filter wheel led to the use of only the sapphire filter throughout the TEM-1 flight.

It should be pointed out that Figures 12, 13, and 14 were obtained from assembled instruments and not from component response curves. Therefore, any shifts or broadenings of the interference filter curves are observed. These modifications of interference filter response curves may occur in our relatively low f/number instruments due to the large ray angles involved.

The relative sensitivity of the spectrograph is largely determined by the CsTe photocathode of the digicon. The wavelength ranges and sensitivities are given in Table 2.

3.5 Dynamic Range and Linearity

The typical dynamic range of a 10 by 10 digicon diode element is shown in Figure 15. The output from one pixel is plotted against the intensity observed by the beam probe photomultiplier. The incident beam intensity was attenuated with neutral density filters. The digicon can be linear over about four decades, depending on the dark count rate. Significant nonlinearity is seen at count rates greater than about 2.5×10^4 counts per sec, as shown in the figure. The response is essentially saturated at 10^5 counts per second. Corrections can be made in the nonlinear range, but this is less satisfactory as saturation is approached. The range of linearity is less than for a typical photomultiplier, but generally larger than that of other available UV imaging sensors. The linearity of the beam probe photomultiplier was established in this range by separate tests. The curve in Figure 15 refers to the digicon-counting circuit combination as assembled for flight and not to the digicon separately.
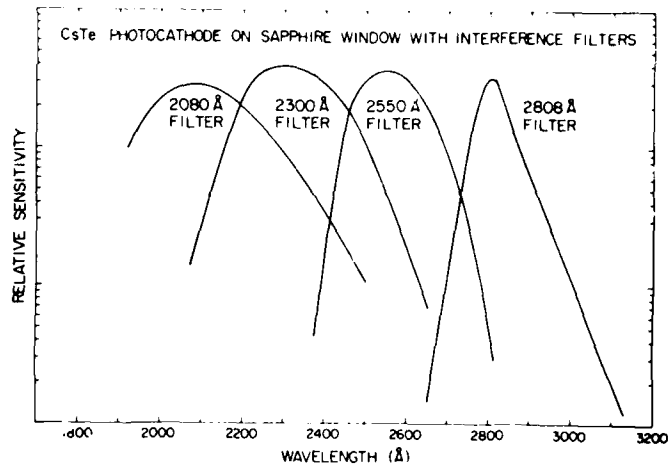
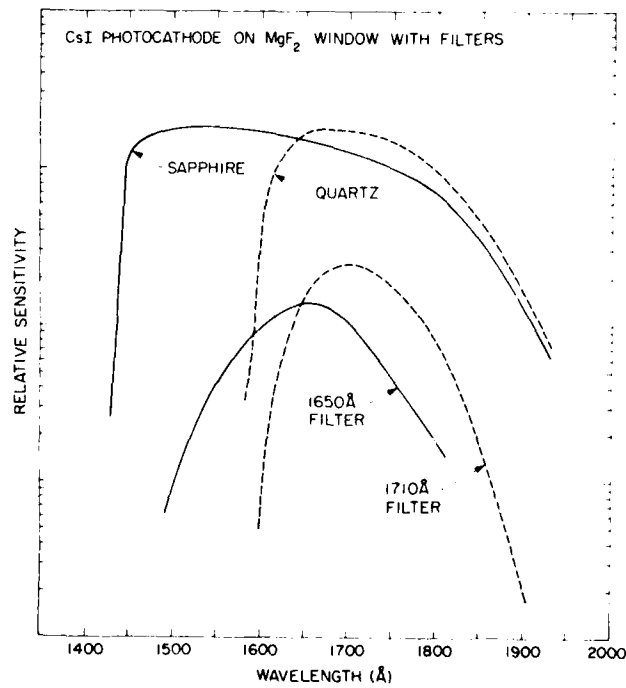Figure 13. Measured Filter Relative Sensitivities for MSP-32

Figure 14. Measured Filter Relative Sensitivities for HSP-52

26

Table 2. Ultraviolet Spectrograph Wavelength Ranges, TEM-1
(Table correct for a point source on optic axis; pixel range is
3.4 times larger for a source that fills the FOV)

Pixel Number	Center Wavelength Å	Pixel Range Å	Relative Response $(phot/s-cm^2-Å-count)$	Comments
0	1123	35*	1.00	---
1	1160	38*	0.93	Unusable
2	1198	40*	0.86	---
3	1239	42	0.80	---
4	1282	44	0.74	---
5	1327	45	0.69	---
6	1373	47	0.64	---
7	1421	49	0.59	Unusable
8	1470	50	0.55	---
9	1521	51	0.51	Unusable
10	1572	52	0.47	Unusable
11	1625	53	0.44	---
12	1678	54	0.41	---
13	1732	55	0.38	---
14	1787	55	0.36	---
15	1843	55	0.33	Over responsive
16	1898	56	0.31	Unusable
17	1954	56	0.29	---
18	2010	56	0.28	---
19	2066	56	0.26	Unusable
20	2121	55	0.25	---
21	2177	55	0.24	Unusable
22	2232	55	0.23	---
23	2286	54	0.22	---
24	2339	53	0.21	---
25	2392	52	0.21	Unusable
26	2443	51	0.21	---
27	2494	50	0.21	---
28	2543	49	0.21	---
29	2591	47	0.22	---
30	2637	45	0.22	---
31	2682	44	0.23	---
32	2725	42	0.24	---
33	2766	40	0.25	Unusable
34	2804	38	0.27	---
35	2841	35	0.29	Unusable

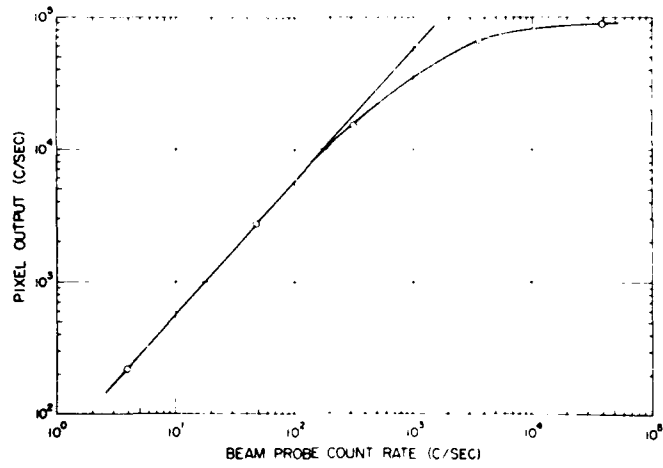*Active width of pixel is one-half of range given equally divided on either side of center wavelength.

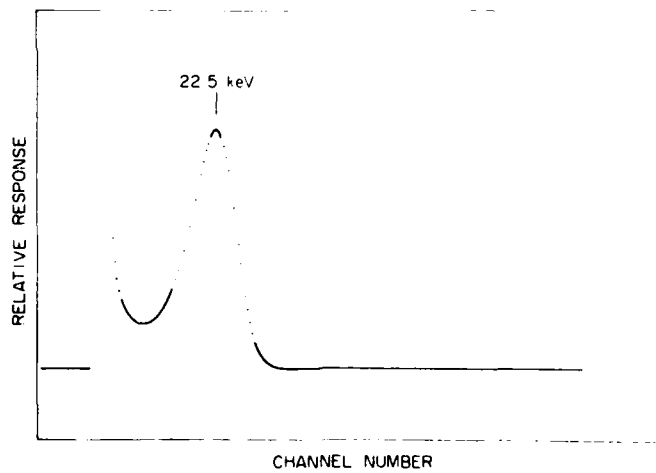Figure 15. Response of Digicon Diode Element at High Count Rates

Figure 16. Pulse Height Distribution of Digicon Diode Element

28

The digicon has a good pulse height distribution for counting systems as shown in Figure 16, which is for a typical diode element with low dark count and average sensitivity. The peak in the distribution is equivalent to 22.5 kV with an applied voltage of about 25 kV. The balance is lost in passage of the photoelectron through a silicon oxide passivation layer and an aluminum layer before being stopped in the silicon diode. The relatively broad minimum on the low energy side makes the location of the discriminator voltage level less critical.

4. FLIGHT SUMMARY

The TEM-1 launch occurred on 10 Nov 1977 at 2100 Mountain Standard Time (MST) from the White Sands Missile Range. The launch was at night with the moon well below the horizon. Additional details are given in Table 3.

Table 3. Flight Summary Data for TEM-1 Flight

Launch date, time	10 Nov 1977, 2100 MST (UT 0400, 11 Nov 77)
Launch location	White Sands Missile Range: 32.4^{o}N, 106.3^{o}W
Solar zenith angle	139.0^{o}
Solar azimuthal angle	258.4^{o}
Exospheric temperature	825K
HLyα solar flux	4.0×10^{11} photon cm^{-2} sec^{-1}
Flight vehicle	Aries (Space Vector Corp.)
VUV/UV data start	t + 155 sec (176 km altitude)
VUV/UV data stop	t + 450 sec (65 km altitude)

The performance of the Aries booster was within the expected range. The altitude versus time is shown in Figure 17 for the sensor module. The observations reported here were between flight times of 155 and 450 sec, which are the high voltage "on" and "off" command times. These times correspond to altitudes of about 176 and 65 km on the up- and down-legs of the flight, respectively.
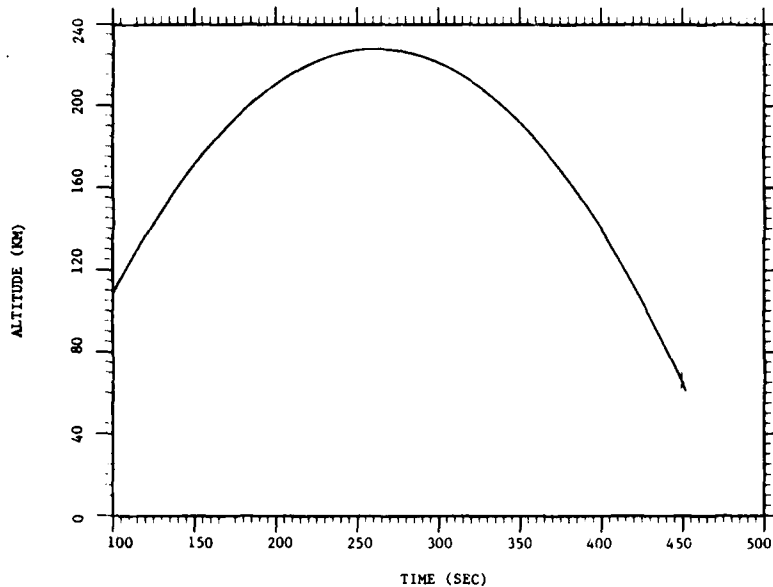
Figure 17. Sensor Altitude vs. Time for the MSMP TEM-1 Flight

The attitude control system of the sensor module did not operate properly in flight, resulting in unplanned movement of the instrument FOV through lower elevation angles and toward the south rather than the north. The post-flight interpretation of the telemetered gyro data coupled with on-board television observation of the earth horizon and observation of VUV stars with the HSP has led to a determination of the pointing directions.[7] These calculations are summarized in Figures 18 and 19, which give the elevation and azimuth of the sensor line of sight plotted against flight time. The instrument line-of-sight (LOS) direction is still believed to have a residual uncertainty of $\pm5^{\circ}$ in azimuth and elevation. The rapid and oscillatory movement of the line of sight prevented the VUV and visible region cameras on board from obtaining photographs of star fields. From the information now available, including the VUV/UV sensor responses, it is possible to identify earth horizon crossings. Further consideration of the data as discussed later in this report helps to refine knowledge of the LOS direction at times near horizon observations.

---

7. The initial analysis of the attitude control system records and determination of pointing direction was made by AFGL (SU) and Boston College. Figures 18 and 19 have been adjusted based on the additional observations mentioned in the text.
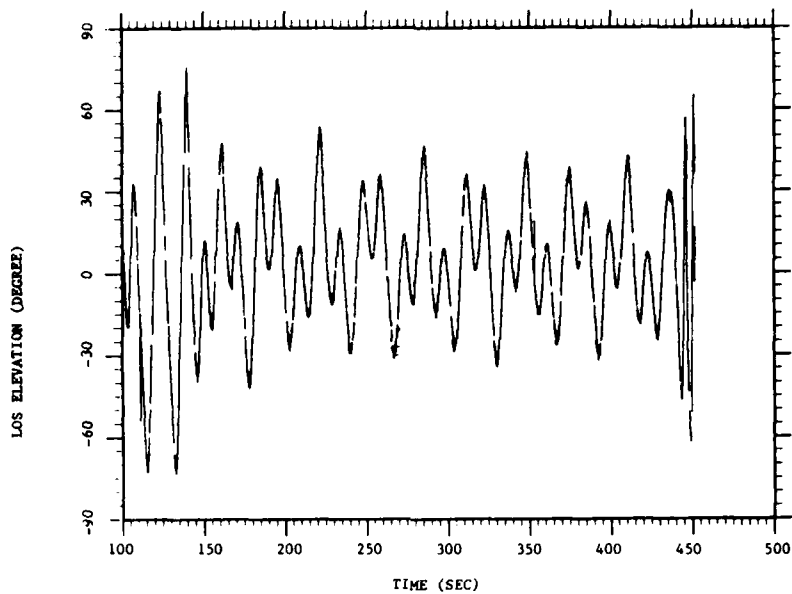
30

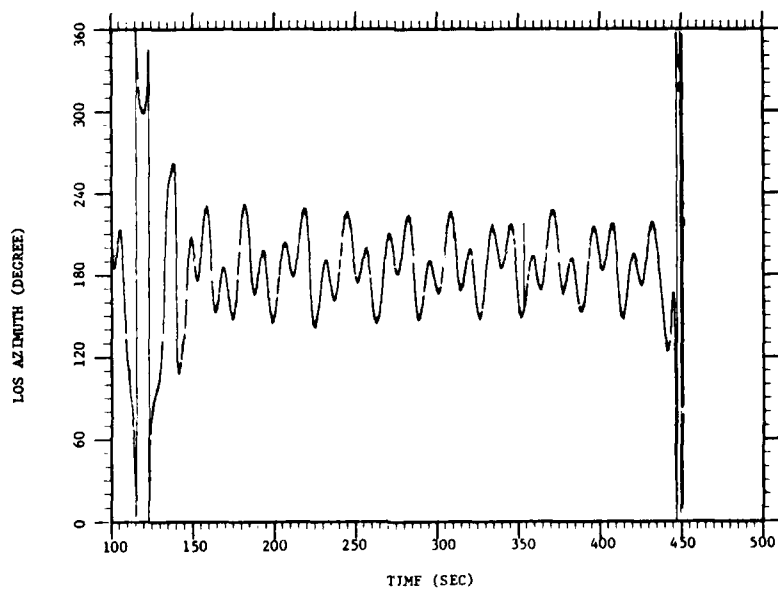Figure 18. Line of Sight Elevation Angle vs. Time for the MSMP
TEM-1 Flight

Figure 19. Line of Sight Azimuth vs. Time for the MSMP
TEM-1 Flight

31

5. AIRGLOW AND ATMOSPHERIC LIMB OBSERVATIONS

5.1 Hydrogen Lyman Alpha (1216 Å)

There is a sizable radiance due to multiple scattering of solar Lyman alpha radiation in both the day and night upper atmosphere. The radiation is scattered around the earth by the small number density of hydrogen atoms in the earth's geocorona, so that night background levels are roughly only an order of magnitude less than day levels. In the daytime, the radiance may be as much as 30 kR.

The expected radiance and its variation with line of sight has been described in multiple-scattering models which give the intensity in Rayleighs as a function of altitude, elevation angle of observation, solar zenith and azimuthal angles, solar H Lyman alpha intensity, hydrogen atom density, and exospheric temperature. These have been compared with rocket and satellite observations and are in reasonably good agreement.[8,9] They also agree well with our observations.

The hydrogen Lyman alpha background emission was clearly observed during the TEM-1 flight on filters 1, 2, and 3 of MSP-11 and on the expected diode elements of the spectrograph. The observed counts were well above the dark count during the flight. The measured radiance ranged between 1 and 4 kR.

The measurements on the three filter positions of MSP-11 were consistent with each other within the larger random scatter on filters 2 and 3. The filter 2 counts appear to be entirely due to H Lyman alpha when the FOV does not include bright stars or the earth's atmospheric limb. Filter 3 is an interference filter of considerably lower sensitivity than filter 1 with its transmission peak at 1216 Å. The ratios of sensitivities of filters 1, 2, and 3 are 1.0, 0.066, and 0.083 at 1216 Å. The spectrograph diodes near 1216 Å are either inoperative or have high noise count levels. The further discussion of Lyman alpha observations will be restricted to MSP-11, filter 1 and MSP-11, filter 3.

The unplanned nature of the changes in LOS direction, together with the filter position changes, results in more or less random LOS directions for data using a given filter. The uncertainty in pointing direction is also a problem, but it is less serious for H Lyman alpha than for the other airglow emissions to be discussed, where an accurate tangent altitude is needed to facilitate the analysis. The filter changes every 0.6 sec so that a given filter only collects data for 0.5 sec out of the total 2.4 sec cycle period for the four filters. The gaps in the coverage with

8. Meier, R.R., and Mange, P. (1970) Geocoronal hydrogen: An analysis of the Lyman alpha airglow observed from Ogo-4, Planet. Space Sci. 18:803.

9. Meier, R.R., and Mange, P. (1973) Spatial and temporal variations of the Lyman alpha airglow and related atomic hydrogen distributions, Planet. Space Sci. 21:309-327.

a given filter require utilization of as much of the flight period as possible, in order to obtain a wide range of viewing conditions.

Initial examination of the observations and the radiance model has led to the use here of data taken between 200 km and the maximum altitude of slightly less than 230 km. In this altitude range, the H Lyman alpha radiance variation with altitude is predicted to be small. The flight time above 200 km altitude extends from about 185 to 340 seconds (Figure 17).

The flight observations are compared with model calculations[10] approximating the conditions of the TEM-1 flight. The exospheric temperature used in the model calculations was 850 K while the actual value during the flight was calculated to be 825 K. The H Lyman alpha flux from the sun was about 4.0×10^{11} photon cm^{-2} sec^{-1} as determined from Atmospheric Explorer data,[11] while a value of 3.75×10^{11} photon cm^{-2} sec^{-1} was used in the model calculations. During the short duration of the flight, the solar zenith angle remained constant at about 139°. The observed values and comparisons with the model are shown in a series of figures, with the observations shown as points and the model calculations as lines.

The variation with azimuth angle between the LOS and the sun is shown in Figures 20, 21, 22, and 23. The observations are grouped into the two elevation angle ranges of 0 to 40° and -20 to -30°. As will be apparent later, the variation with elevation angle between 0 and -20° is too large to allow a comparison in this manner. For the 0 to 40° ranges, the observations are about 25 percent larger than the model, but the trend toward larger radiance values at smaller azimuth angles is evident. This is considered satisfactory agreement considering the uncertainties involved. For the -20° to -30° elevation range, there is excellent agreement with the model. As can be seen from the figures, the azimuthal angle range was about 90°.

The radiance variation with elevation angle is shown in Figures 24, 25, 26, 27, 28, and 29. Three ranges of solar azimuth angle have been used: 85° to 95°, 75° to 85°, and 30° to 40°. The measured radiance decreases as the elevation angle drops below zero, and it matches the model values fairly well at negative elevation angles. However, the relative change is larger than the model prediction, since the observed radiance is larger than the model values for the upward looking observations. Again the agreement is generally satisfactory considering the uncertainties involved. The absence of points at elevation angles below -10° for the 30° to 40° azimuth range is due to the lack of observations under these conditions during the unplanned movements of the LOS as discussed in Section 4.

---

10. Meier, R.R. (1979) Personal communication.
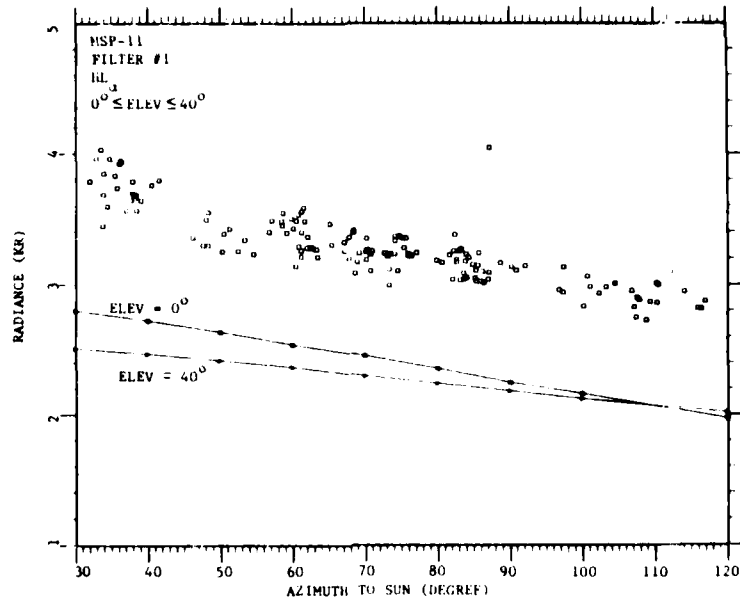11. Hinteregger, H. (1979) Personal communication.

Figure 20. Hydrogen Lyman Alpha Radiation Recorded by MSP-11, Filter 1 for Elevation Angles Between 0° and 40°
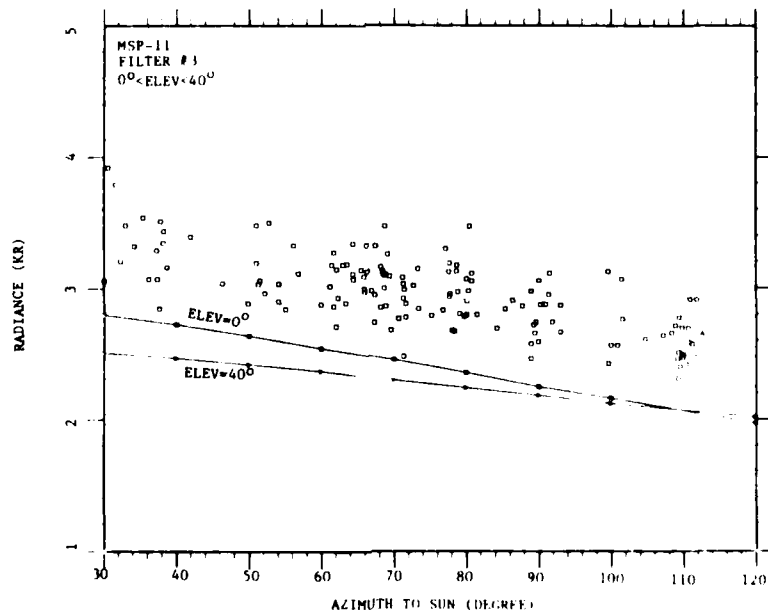

Figure 21. Hydrogen Lyman Alpha Radiation Recorded by MSP-11, Filter 3 for Elevation Angles Between 0° and 40°
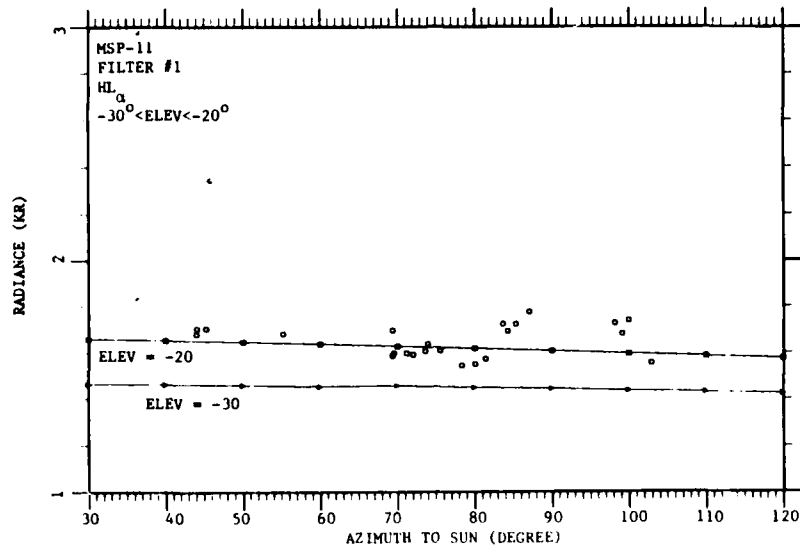
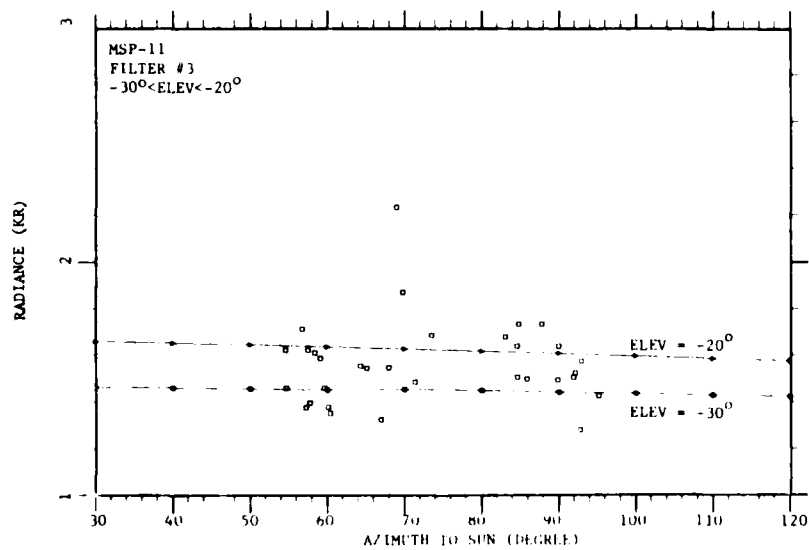Figure 22. Hydrogen Lyman Alpha Radiation Recorded by MSP-11, Filter 1 for Elevation Angles Between -30° and -20°

Figure 23. Hydrogen Lyman Alpha Radiation Recorded by MSP-11, Filter 3 for Elevation Angles Between -30° and -20°

Figure 24. Hydrogen Lyman Alpha Radiation Recorded by MSP-11, Filter 1 for Solar Azimuth Angles Between 85° and 95°

Figure 25. Hydrogen Lyman Alpha Radiation Recorded by MSP-11, Filter 3 for Solar Azimuth Angles Between 85° and 95°

Figure 26. Hydrogen Lyman Alpha Radiation Recorded by MSP-11, Filter 1 for Solar Azimuth Angles Between 75° and 85°

Figure 27. Hydrogen Lyman Alpha Radiation Recorded by MSP-11, Filter 3 for Solar Azimuth Angles Between 75° and 85°
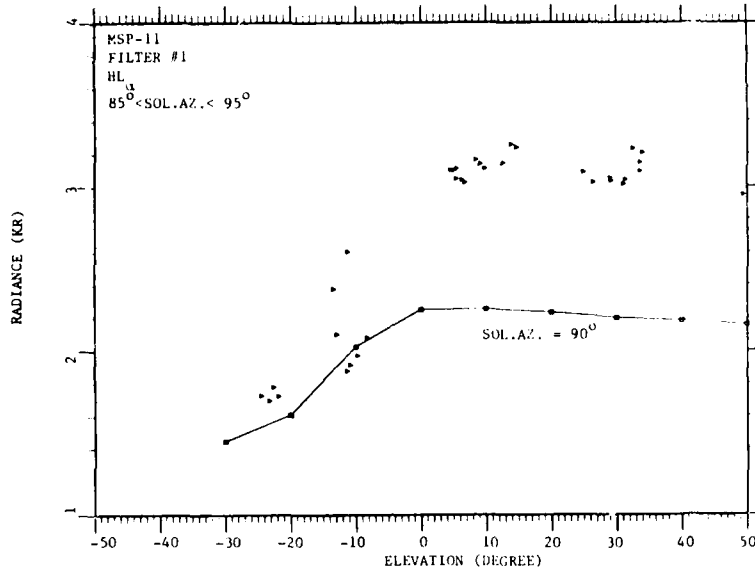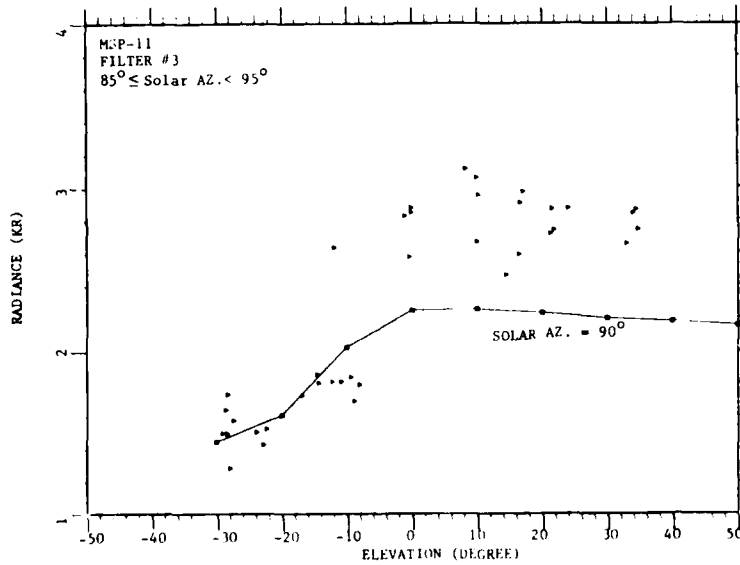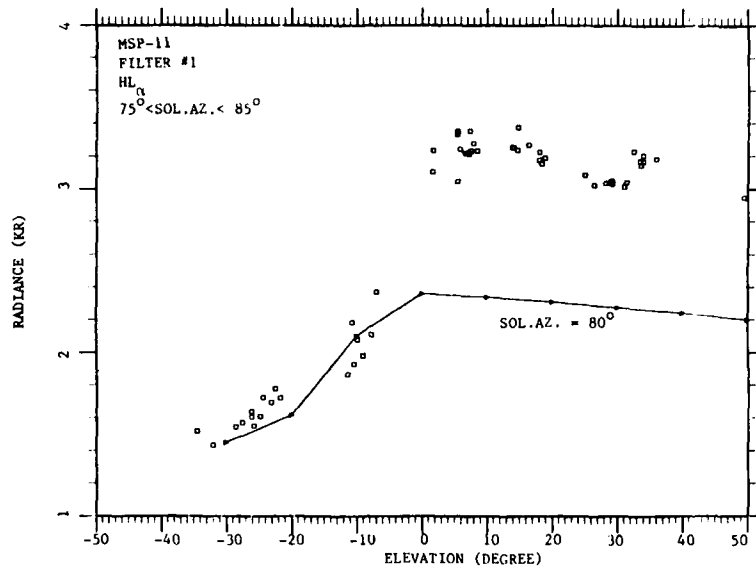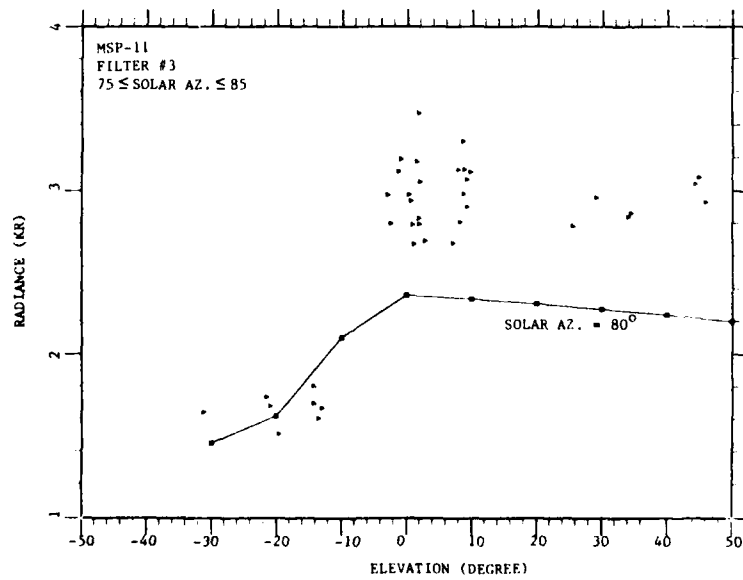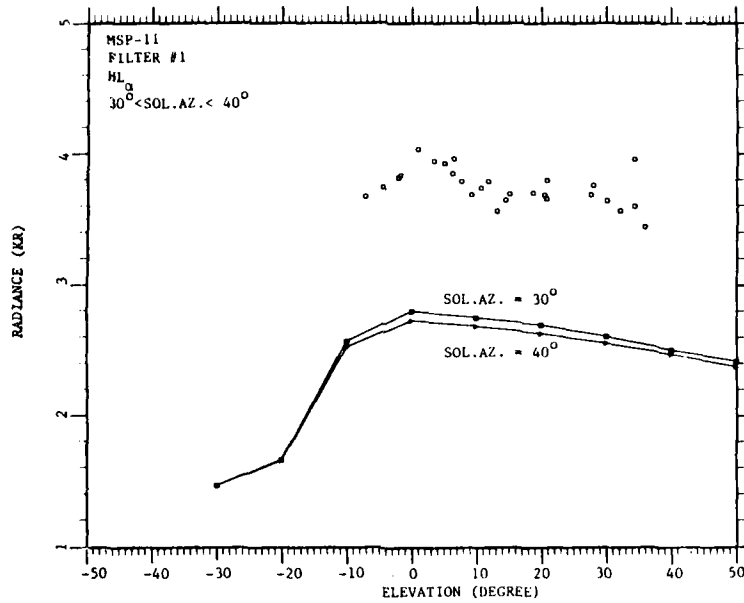
37

Figure 28. Hydrogen Lyman Alpha Radiation Recorded by MSP-11, Filter 1 for Solar Azimuth Angles Between 30° and 40°
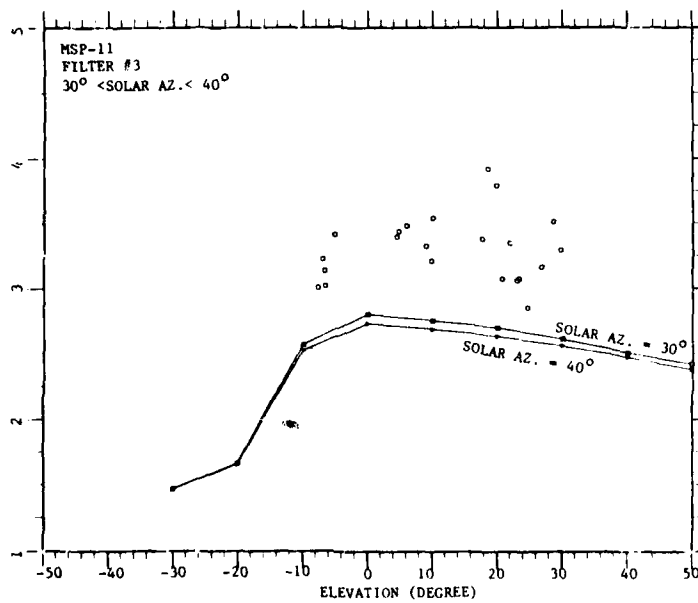

Figure 29. Hydrogen Lyman Alpha Radiation Recorded by MSP-11, Filter 3 for Solar Azimuth Angles Between 30° and 40°

38

Observations using filters 1 and 3 are in reasonably good agreement and exhibit no discernible trends when compared in the solar azimuth and LOS elevation groups shown in Figures 20 to 29. Filter 1 covers a wider wavelength interval than filter 3, as shown in Figure 7. Therefore, it is unlikely that any source of radiation other than hydrogen Lyman alpha makes a significant contribution. The observations were also examined for possible stellar interference and none was found.

The generally good agreement between observations and model calculations found for the hydrogen Lyman alpha radiance lends credence to the observations and models. It also gives support to use of these models in the interpretation of field observations of 1216 Å radiation.

5.2 Molecular Oxygen Herzberg Bands (2500 to 2800 Å)

Emission from the Herzberg bands of molecular oxygen can be observed during movements of the line of sight through the atmospheric limb of the earth. There were about 20 of these unplanned limb crossings during the course of the flight. The geometry is shown in Figure 30. As the line of sight moves toward the position of the earth, the tangent altitude Z_o, or distance of closest approach of the line of sight to the earth, varies from the sensor module altitude to zero. When the LOS passes through the earth's atmospheric limb, the path length through an atmospheric layer is greater than for zenith or nadir viewing, with the results that more emitting species will be in the field of view. For optically thin emission under consideration here, a maximum is seen in the radiance versus tangent altitude plot when the radiation is emitted from a limited altitude region.

Well developed maxima are observed in radiance vs. tangent altitude plots for seven adjacent pixels in the spectrometer and for MSP-32, filters 3 and 4. The spectrometer pixels are 27, 28, 29, 30, 31, 32 and 34. Pixels 33 and 35 are not usable. As can be seen from Table 2 and Figure 13, the wavelengths involved are between about 2500 and 2800 Å, which are in short wavelength end of the Herzberg bands $O_2(A^3\Sigma_u^+ \to X^3\Sigma_g^-)$ resulting from atomic oxygen recombination in the night atmosphere. This recombination is known to occur in a layer whose volume emission rate is centered near 92 km in the atmosphere.[12, 13] The bands are difficult or impossible to observe in the daytime due to solar Rayleigh scattering and thus have been observed only at night.

The spectrometer observations are shown in Figures 31 to 37. The data have been smoothed by performing a sliding average with a 10 km averaging window.

12. Packer, D.M. (1961) Altitudes of the night airglow radiations, Ann. Geophys. 17:67.

13. Reed, E.I. (1968) A night measurement of mesospheric ozone by observations of ultraviolet airglow, J. Geophys. Res. 73:2951.
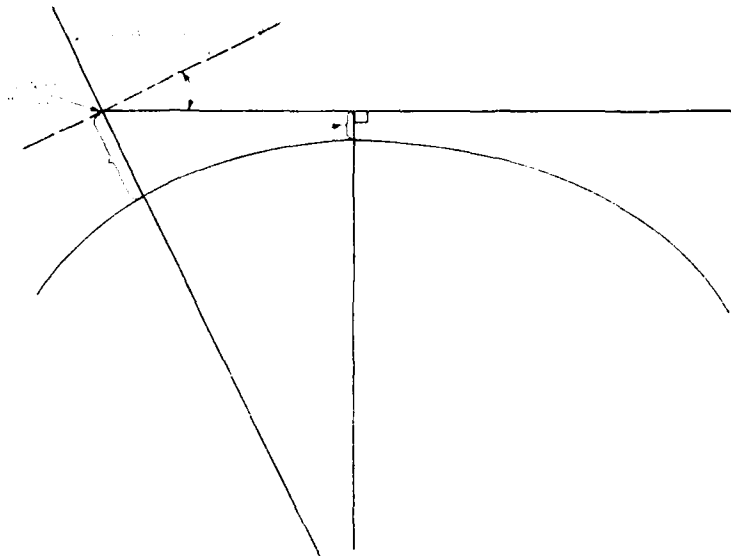
Figure 30. Geometry of an Earth Limb Scan Showing Sensor
Module at Altitude Z with Elevation Angle θ and Corresponding
Tangent Height, Z_0

Figure 31. Ultraviolet Spectrometer Data as a Function of
Tangent Height for Detector 27, Center Wavelength 2494 Å

40

Figure 32. Ultraviolet Spectrometer Data as a Function of
Tangent Height for Detector 28, Center Wavelength 2543 Å

Figure 33. Ultraviolet Spectrometer Data as a Function of
Tangent Height for Detector 29, Center Wavelength 2590 Å

41

Figure 34. Ultraviolet Spectrometer Data as a Function of
Tangent Height for Detector 30, Center Wavelength 2637 Å

Figure 35. Ultraviolet Spectrometer Data as a Function of
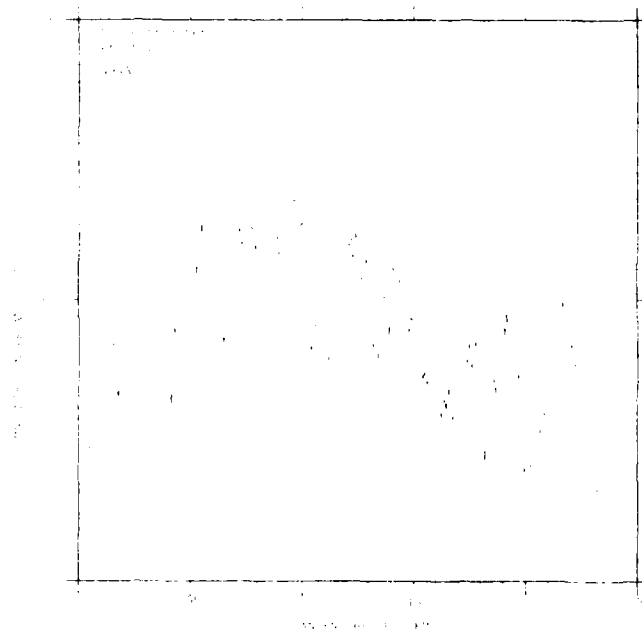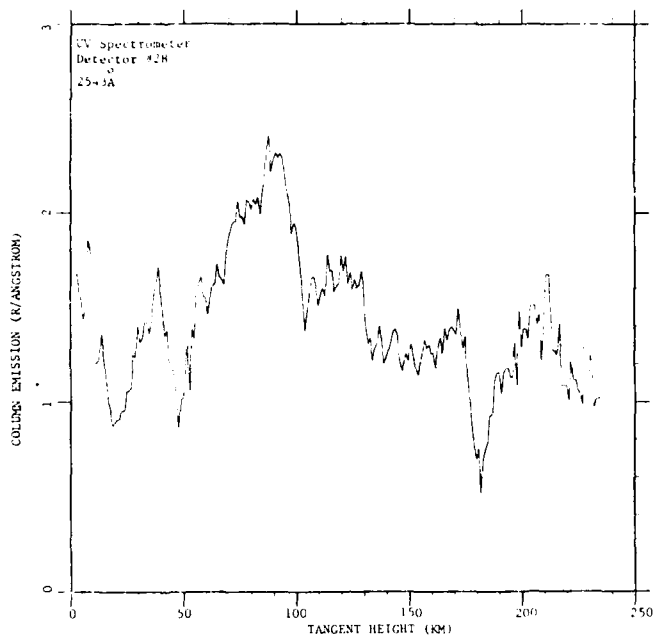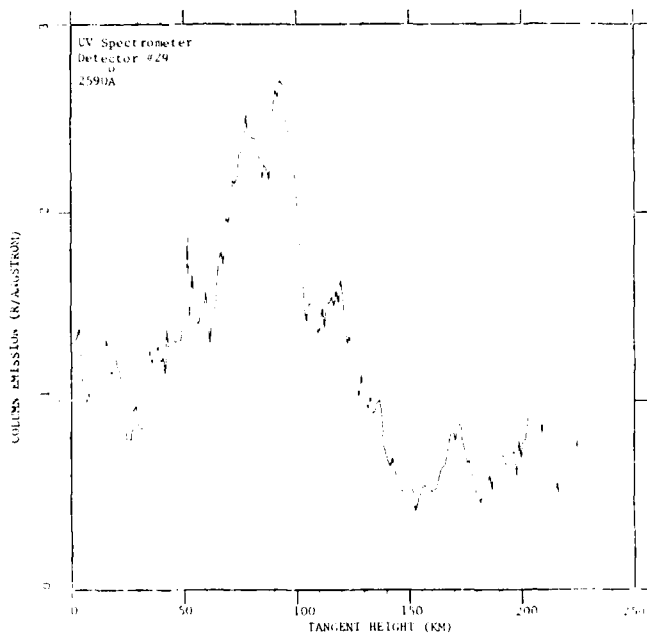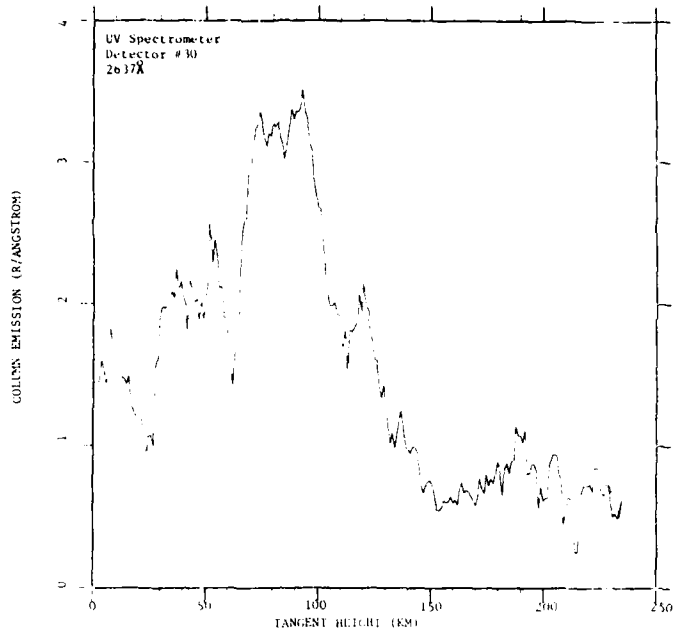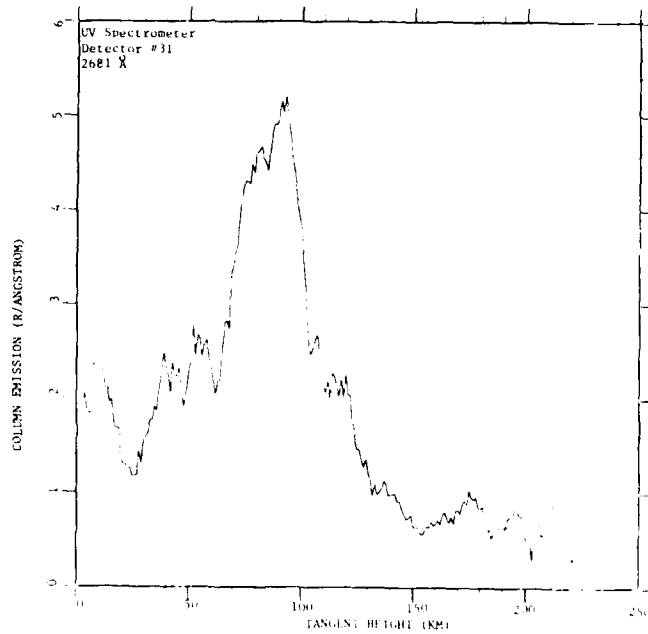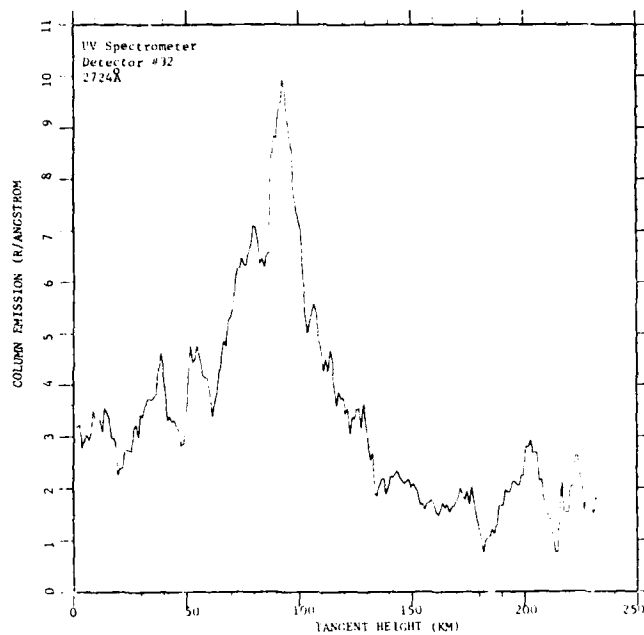Tangent Height for Detector 31, Center Wavelength 2681 Å

42

Figure 36. Ultraviolet Spectrometer Data as a Function of
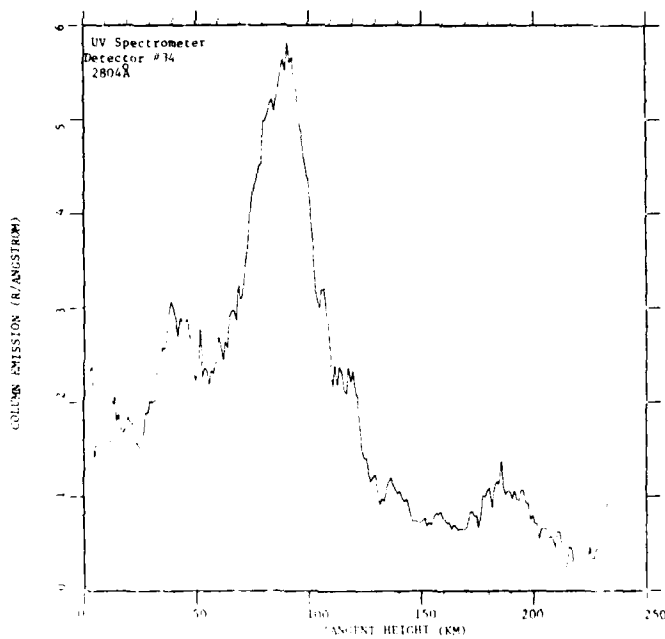Tangent Height for Detector 32, Center Wavelength 2724 Å

Figure 37. Ultraviolet Spectrometer Data as a Function of
Tangent Height for Detector 34, Center Wavelength 2804 Å

43

The LOS movement occurs rapidly relative to the filter cycle time of 2.6 sec of the photometers and therefore the spectrometer provides considerably more data than MSP-32, since all pixels are obtaining data for every 0.1 sec frame. Thus, more use can be made of the spectrometer data.

The tangent altitudes given in Figures 31 to 37 were not obtained directly from the LOS directions on the MSMP attitude tapes. The residual errors in the elevation coupled with the sensitivity of tangent altitude to elevation angle (about 15-20 km/degree of elevation for altitudes of concern here) made another procedure necessary. To calculate the tangent height at any given time, both the sensor altitude and the elevation angle of the LOS are needed. In this case, it was more convenient to correct the calculated tangent height than to correct the elevation itself. The correction was based on the data from the HSP, which will be discussed in detail in the next section. The response of this instrument to the airglow layer was so sharp and prominent that each earth limb scan could be plotted individually with a signal-to-noise ratio greater than 10. We assume that this signal arises from a narrow atmospheric layer whose altitude is constant. Using the uncorrected elevation angle to compute tangent heights, one notes that the irradiance versus time data from the HSP was transformed to irradiance versus tangent height for each individual limb scan. One of these was chosen arbitrarily as a reference, and tangent height differences were measured by overlaying the other scans on the reference scan. Applying these corrections to each tangent height scan then resulted in a corrected tangent height versus time data base for the entire flight. An absolute error still remained at this point, but it was the same for all scans. It was then possible to transform the data from the other instruments from irradiance versus time to irradiance versus tangent height, making use of all of the data to obtain the best possible statistics.

Fixing the absolute tangent height scale was the remaining problem. Previous measurements by others[12, 13] of the volume emission rate of the Herzberg bands of molecular oxygen seemed to be the most reliable means of providing the final correction. The emitting layer has a volume emission rate maximum at 93 km, and this leads to a maximum column emission at a tangent height of 90 km. Figures 31 to 37 have therefore been shifted so that the observed maxima are at 90 km.

Turning now to the shapes and intensities of the Herzberg band profiles in Figures 31 through 37, one will notice that the intensity increases between about 2500 Å and the end of the measurement range at about 2800 Å. There is considerable scatter in the observations even after the averaging procedures described, and the tangent height profiles are rather indistinct in the shorter wavelength data. The peaks are unmistakable at the longer wavelengths, however. This intensity

distribution matches in a general way that expected from the Herzberg bands. The spectrometer wavelength ranges and relative sensitivities are given in Table 2.

The spectral intensity distribution is shown in Figure 38, which displays the peak radiance values from the tangent height curves of Figures 31 through 38 against the wavelength range of each pixel after subtraction of the background levels observed above 150 km tangent height. Herzberg band spectra observed at night with the downward looking satellite experiment[5] Vacuum Ultraviolet Backgrounds, (S3-4), are shown in Figure 39. The upper right-hand corner also
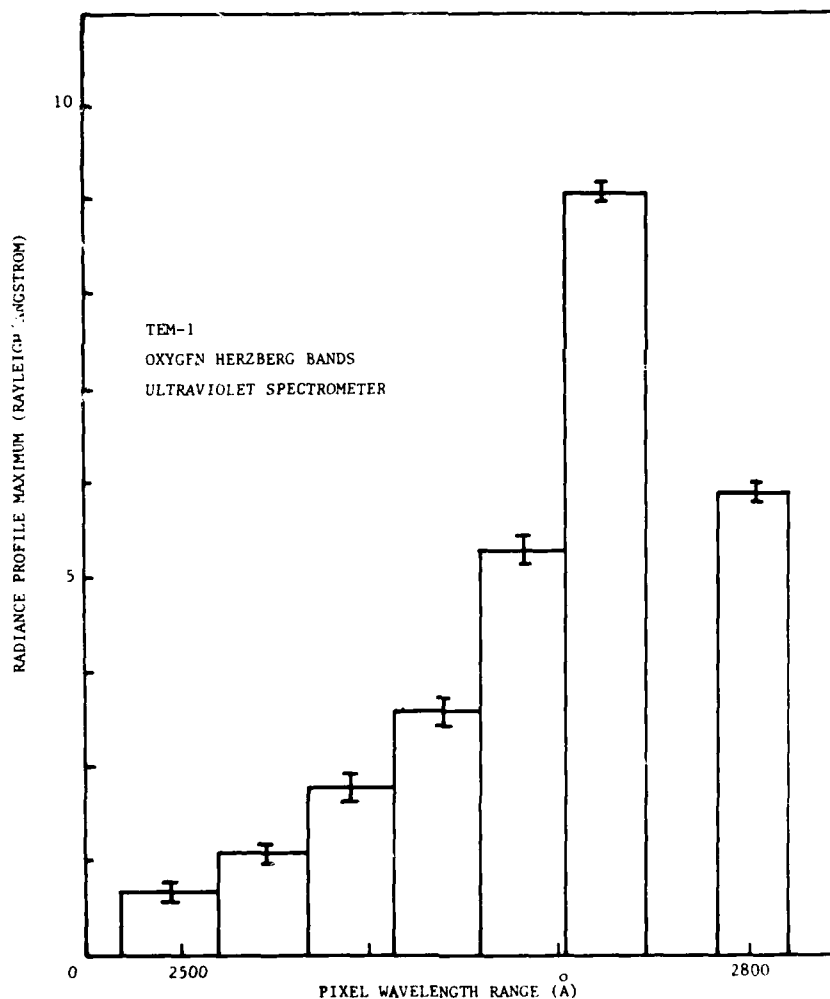
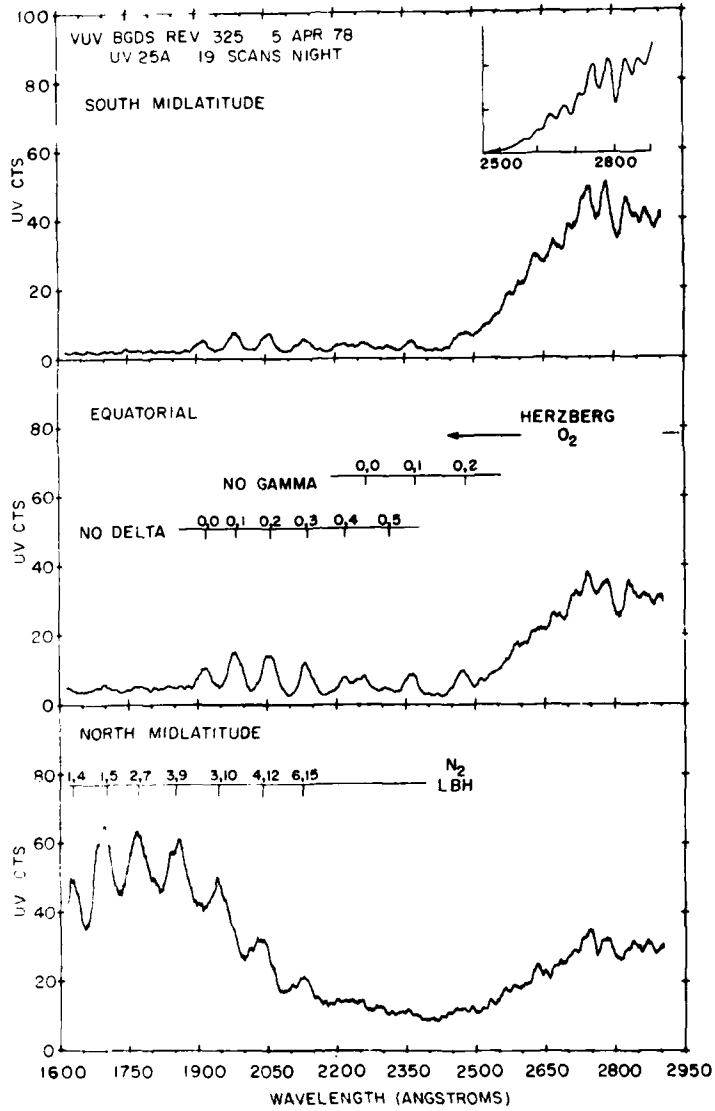Figure 38. Spectrum of the Herzberg Bands Derived From the Data in Figures 31 to 37

45

Figure 39. Night Ultraviolet Spectra From S3-4 Satellite
Experiment, Vacuum Ultraviolet Backgrounds. Note Herz-
berg bands of O_2 in 2500-2900 Å region (Ref. 1-5)

shows a laboratory spectrum. All of these spectra are obtained at a bandwidth of 25 Å, which is smaller than the UV spectrometer bandwidth of 40 to 50 Å (Table 2). When allowance is made for this difference, the similarity in the wavelength distributions between 2500 and 2800 Å is apparent. The pronounced dip at 2800 Å appears to be reflected in the TEM-1 data.

The intensity of the TEM-1 radiation is within the range of natural variability found for the oxygen Herzberg bands. With integration of the maximum radiance level values given in Figure 38 over the 2500 to 2800 Å range, a total value of about 1270 Rayleighs is found for the maximum of the tangent altitude data. However, for comparison with other observations, it is necessary to convert this value from the horizon maximum value to the nadir or downward looking value. This has been done by using previously observed volume emission rates[12, 13] to calculate a limb brightening factor of 30, which is the ratio of the maximum radiance to the nadir value. Therefore, the observed nadir value is 1270 ÷ 30 or about 42 Rayleigh. Satellite observations covering several months[14] find a wide range of Herzberg band intensities over the 2500-2800 Å region, with most of the observations falling between 45 and 150 Rayleigh. Thus, the TEM-1 observations are at the lower end of this range. The S3-4 observations[5] in Figure 39 are larger than the TEM-1 observations, but are also within the previously observed range.[14] The upper spectrum for the south midlatitude region in Figure 39 has a radiance of about 130 Rayleigh in the 2500 to 2800 Å region. The equatorial and north midlatitude spectra are weaker, as can be scaled from the figure.

The combination of the wavelength distributions observed by both the spectrometer and MSP-32, filters 3 and 4, together with the intensity, leaves no doubt that the Herzberg oxygen emission is being observed. Thus, the adjustment of the peaks in the tangent height curves to the values calculated for the Herzberg bands is justifiable. It is clear, however, that more direct observations of the earth limb with accurate knowledge of the pointing direction would be very useful.

Finally, it is possible to observe the Herzberg band airglow layer using the spatial resolution available from the 10 × 10 element digicon on MSP-32. Figure 40 illustrates this observation. The green-line (5577 Å) airglow layer is seen in television camera frames during excursions of the line of sight near the earth. The position of this layer in the TV image, shown by the solid line, matches in a general way the pixels showing the brightest intensity across the digicon. Both types of emission are produced by oxygen atom recombination and are known to originate at approximately the same altitude. This correlation also demonstrates the use of the 10 × 10 digicon to obtain spatially imaged data.

---

14. Reed, E. I. , and Chandra, S. (1975) The global characteristics of the atmospheric emissions in the lower thermosphere and their aeronomic implications, J. Geophys. Res. 80:3053-3062.
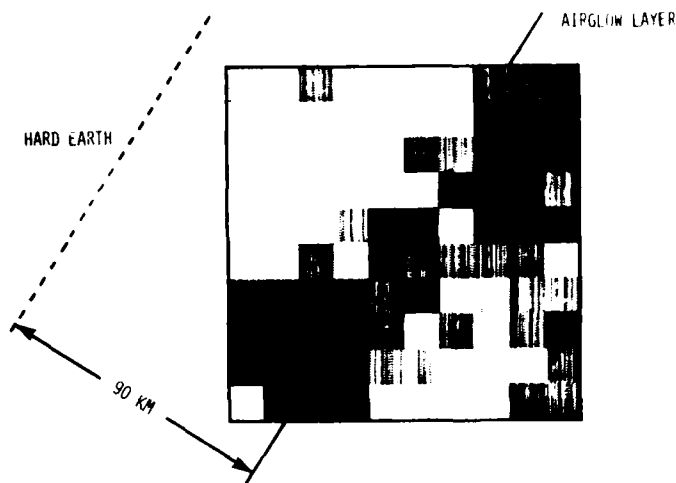
Figure 40. Density Plot of $4^O \times 4^O$ Spatial Data of MSP-32, Filter 4 at Mission Time 278.4 sec. The position of the airglow layer relative to the instrument field of view was determined by transfer of its image in the on-board television. The position of the hard earth edge (dashed line) was not visible in the TV, but was calculated, based on an assumed airglow altitude of 90 km

5.3 High Sensitivity Photometer Observations of the Airglow

The High Sensitivity Photometer observed an airglow layer with such high signal-to-noise ratio that it was used as a tangent height reference, as described in Section 5.2. The data are shown in Figure 41 as radiance versus tangent height. Finding a satisfactory explanation of these data has been one of the most difficult parts of the UV data analysis. The source of this unexpected radiation cannot be definitely established from the available measurements, but some possibilities can be discussed.

The way in which the final tangent height data base was generated was outlined in Section 5.2. It is still subject to systematic as well as random error, but one thing is certain. Any reasonable method of deducing tangent height from the data will place the HSP limb radiation source and the O_2 Herzberg bands at the same tangent height (compare Figures 41 and 37). Since the O_2 Herzberg bands have been observed many times[13, 14] before, it is not likely that the HSP tangent height is in error by more than 10 km.

This conclusion limits the wavelength range that can be transmitted to the detector. Atmospheric molecular oxygen will completely absorb radiation in the 1400 to 1800 Å region in the Schumann-Runge (SR) continuum. Transmission along the slant path to 90 km is possible only at wavelengths longer than about 1800 Å in
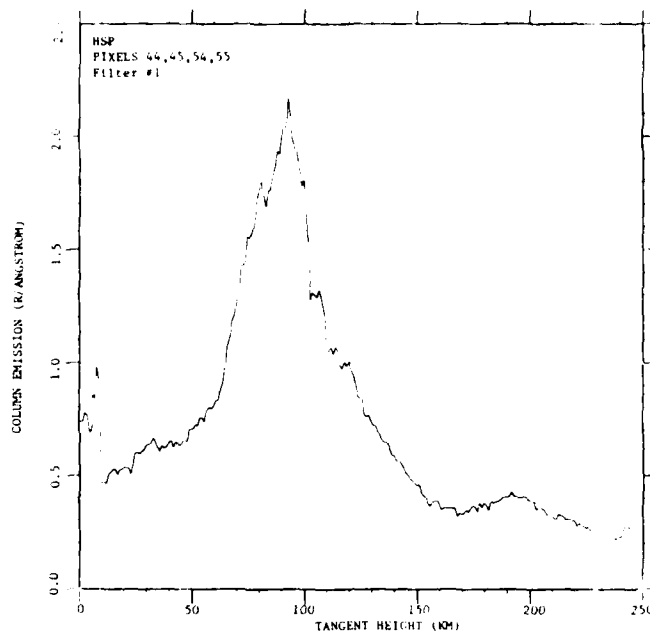
Figure 41. HSP Data as a Function of Tangent Height
for Filter 1. The data of pixels 44, 45, 54 and 55
have been averaged

the SR bands. Therefore, it would appear that the airglow layer is being observed
in the longer wavelength part of the CsI sensitivity curve, as shown in Figure 14
and also Figure 12.

It was not possible to calibrate the HSP in the laboratory prior to flight due to
the delivery date, and Figure 14 is for a similar instrument. The radiance cali-
bration shown in Figure 41 was obtained from the flight data. A total of 16 simul-
taneous observations of stars by the HSP and MSP-11, filter 2 or 4, were made.
In these cases, oxygen absorption was not a problem since the observations were
generally in an upward direction. From the relative count rates of the two instru-
ments, the HSP sensitivity was calculated. This value applies to the most sensi-
tive wavelength region of about 1450 to 1800 Å and thus cannot be used to calculate
limb brightness directly, since oxygen absorption prevents observation at these
wavelengths. Because of these uncertainties, no firm conclusions can be drawn
about radiance values of the HSP airglow peak. The HSP filter wheel was locked
with the sapphire filter in place due to unreliable preflight operation of the wheel,
and all measurements were obtained with the sapphire filter only. All sensors
were destroyed due to a recovery system problem; therefore, no post-flight
calibration was possible.

The only known night airglow emission that the general spectrum [illegible] by the HSP is the molecular nitrogen Lyman-Birge-Hopfield bands seen in a recent AFGL satellite experiment. This emission could be suggested [illegible] since the spectrum (Figure 42 and Figure 39) extends from about 1400 to 2000 Å. This explanation has been considered at length, but it is not possible to reach a firm conclusion for this report because the night LBH has only recently been discovered and its mechanism, altitudinal dependence, and other characteristics are not known. Also, the lack of a laboratory calibration makes any intensity measurement in the CsI tail region uncertain. It is possible that an other unidentified airglow previously unrecognized might be responsible.

Other instruments on HEAO-1 might be expected to observe this emission, providing a cross check. Candidates for such checks are MSP-11 filters 2 and 4, and the spectrometer. MSP-11 filter 2 did in fact observe a radiation source at about the same tangent height as shown in Figure 43. The limb source is to be seen above a steadily increasing background of H Lyman-α radiation to which this filter responds to a small degree (see Figure 12). As with the HSP, the observed limb maximum radiation must be from wavelengths longer than 1800 Å due to oxygen absorption. Intensity measurements must use the tail of the response curve, and it is available only out to about 2000 Å (Figure 12). The MSP-11, filter 4 curve shown in Figure 44 does not exhibit a peak in the limb scan although it matches in a general way the HSP sensitivity curve. The explanation may lie in its much lower absolute sensitivity compared with the HSP or it may be due to the lower relative sensitivity in the long wavelength wing of the interference filter beyond 1800 Å, where the observed HSP emission is thought to be. The data from the spectrometer in the 1450 to 1950 Å region are shown in Figures 45 through 50. Here too, no limb radiation peak is observable, probably due to oxygen absorption. The MSP-32 limb scans exhibit a maximum only for filter 3, which can observe the oxygen Herzberg bands. Also no limb maximum was observed between 1950 and 2450 Å by the spectrometer.

The similarity in tangent altitude and shape between the HSP limb peak and the oxygen Herzberg band limb maxima mentioned earlier suggests an entirely different explanation for the HSP observations. The O_2 Herzberg radiation observed by spectrometer pixel 34 at 2804 Å (Figure 37), for example, is virtually identical to the HSP limb in tangent height profile. This similarity suggests that the HSP might in fact have detected the Herzberg bands. This could happen if its photocathode were CsTe instead of CsI, because the sensitivity of the former extends to at least 3000 Å. A check into the records of the Martin-Marietta Corporation, which built the HSP, and the Electron Vision Corporation, which made the Digicon phototube, indicated that the photocathode was CsI as specified. Confusion between the two types is unlikely, because different deposition processes are used. However,
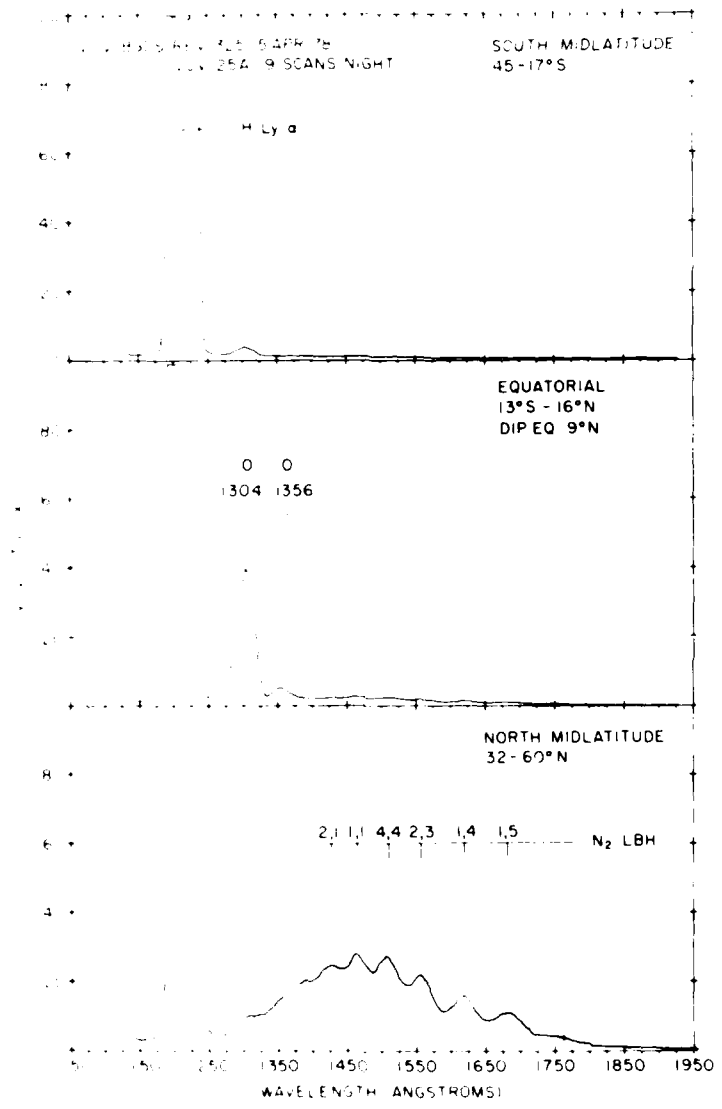
SOUTH MIDLATITUDE
45-17°S

H Ly α

EQUATORIAL
13°S - 16°N
DIP EQ 9°N

O   O
1304 1356

NORTH MIDLATITUDE
32-60°N

2,1 1,1 4,4 2,3 1,4 1,5 _____ N₂ LBH

WAVELENGTH (ANGSTROMS)

Figure 4.   Night Spectra Illustrating N₂ LBH Band Spectra
in the North Mid-latitude Region Data from Vacuum Ultra-
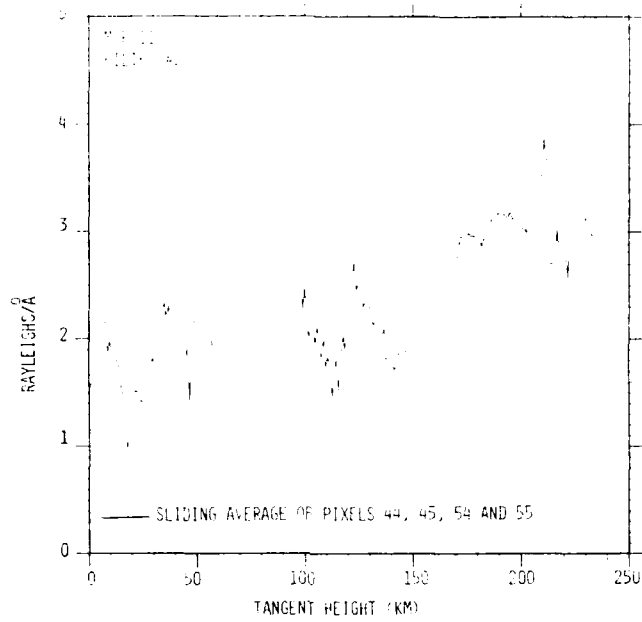violet Backgrounds Experiment on S3-4

51

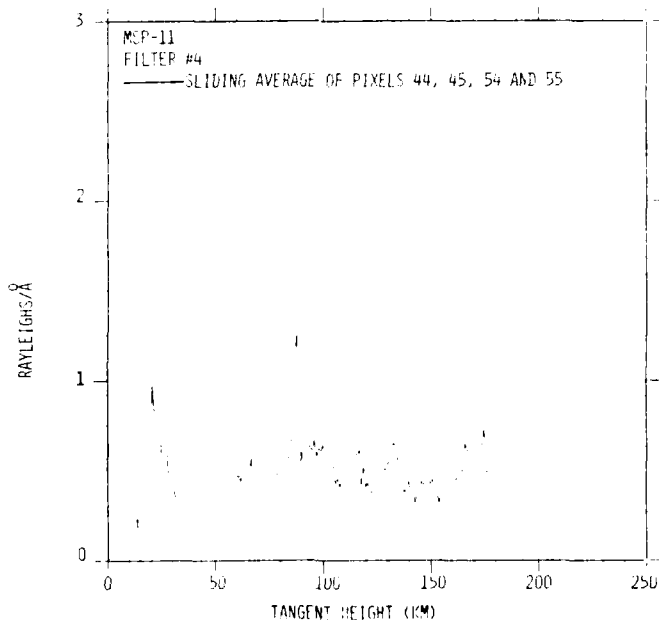Figure 43. MSP-11, Filter 2 Data vs. Tangent Height

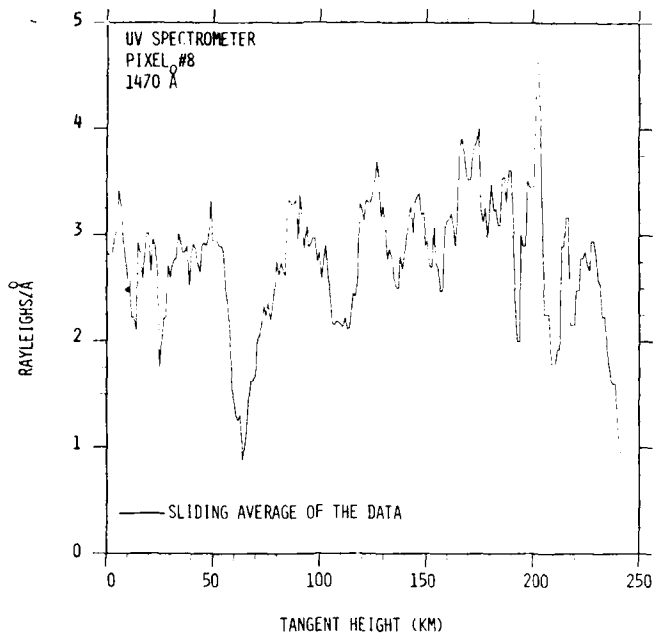Figure 44. MSP-11, Filter 4 Data vs. Tangent Height

Figure 45. Ultraviolet Spectrometer Data at 1470 Å
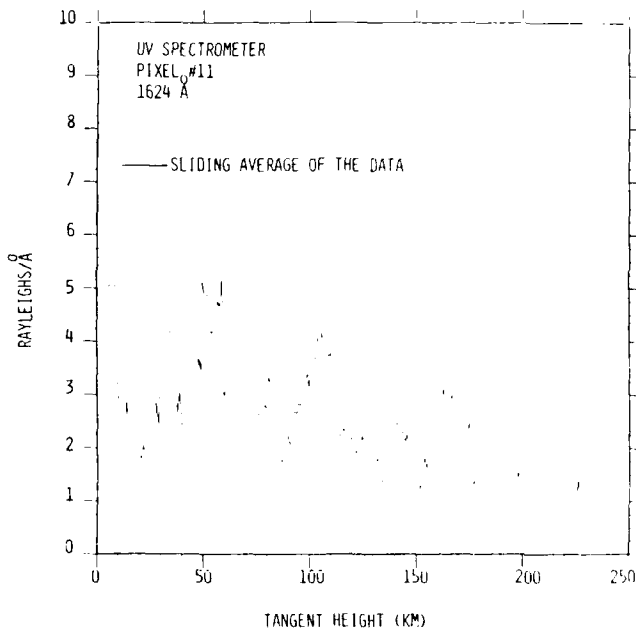vs. Tangent Height

Figure 46. Ultraviolet Spectrometer Data at 1624 Å
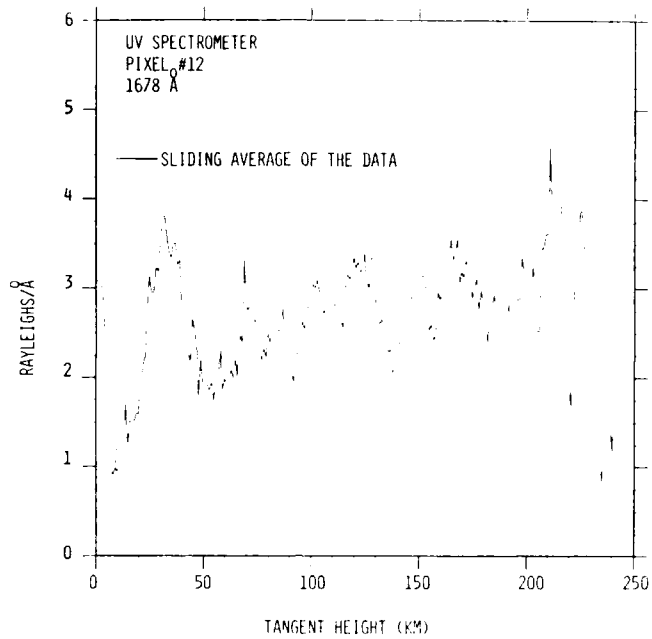vs. Tangent Height

53

Figure 47. Ultraviolet Spectrometer Data at 1678 Å
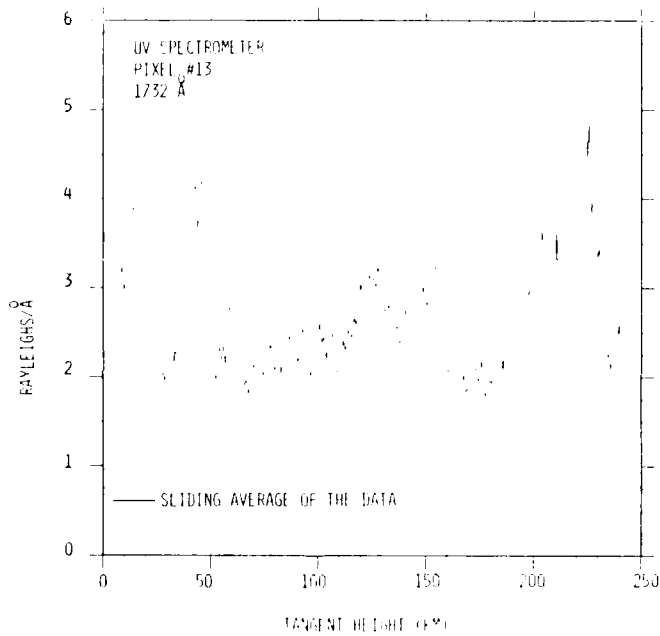vs. Tangent Height

Figure 48. Ultraviolet Spectrometer Data at 1732 Å
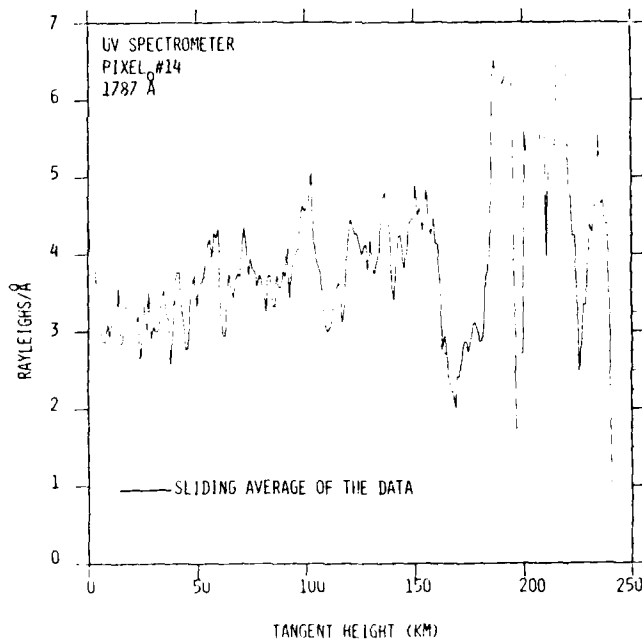vs. Tangent Height

54

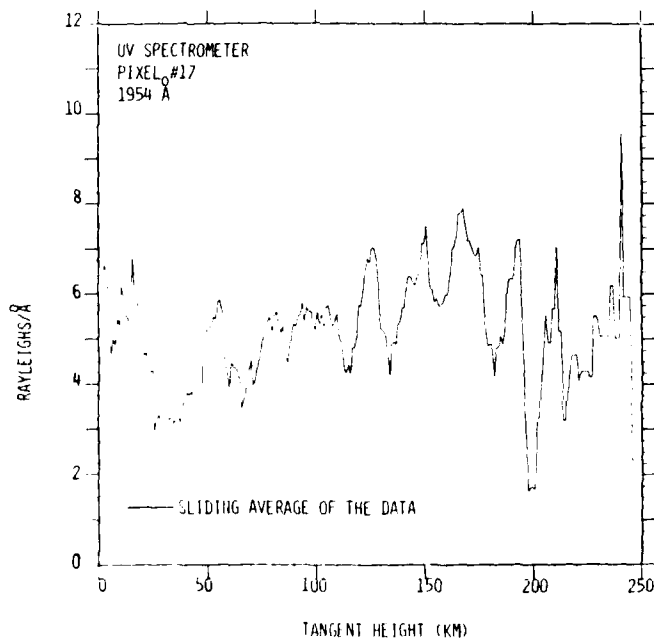Figure 49. Ultraviolet Spectrometer Data at 1787 Å vs. Tangent Height

Figure 50. Ultraviolet Spectrometer Data at 1954 Å vs. Tangent Height

the same vacuum apparatus is used for both types, so some contamination with CsTe is possible (although none has been reported in other CsI cathodes from the Electron Vision facility). Even if this explanation is accepted for the HSP, the problem of explaining the limb maximum on MSP-11, filter 2 would remain. In this case, laboratory calibrations leave no doubt that a CsI photocathode was used on the digicon.

In summary, no completely satisfactory explanation for the HSP limb maximum can be given. Despite seemingly numerous rocket and satellite observations over a period of years, the weak night airglow at these wavelengths has received little attention. Further consideration appears to require additional flight observations.

6. STELLAR OBSERVATIONS

During the flight, at least 69 star sightings were recorded on at least one of the photometers. Due to the tumbling caused by the ACS malfunction, the line of sight is scanning the night sky at rates as high as 20 degrees per second. This motion slews a stellar image across several pixels during each 0.1 second frame. The sum of those pixel counts is used to determine the magnitude of the star in that particular band pass.

Although it is relatively easy to observe stars in the computer printout of the flight data, a relatively simple algorithm was devised to do star searches and to compile the response from those pixels which observed stars. For each 0.1 sec frame the average response and the standard deviation (σ) for all usable pixels was calculated. Then pixels with a response greater than 3σ above the average (called outliers) were identified and the response was printed. The contribution of those pixels were removed from the average and standard deviation and a second search for outliers was performed. The results of this approach were then studied to determine which observations corresponded to behavior expected for response to a star.

The brightest star observed was α-Eridanus at 363.3 sec and again at 424.7 sec. Its celestial coordinates are RA = 24.23^O and δ = 57.35^{O}S, which corresponds to a viewing direction with AZ = 169.96^O, El = -1.17^O; α-Eridanus has been classified[15] as a B9n star with apparent visual magnitude of 0.60. It has been studied previously[16] by instruments on OAO-2, by rocket borne instruments[17] and from Apollo 17.[18]

Because of the large number of references cited above, they will not be listed here. See References, page 59.

Each pixel has a relatively linear response for count rates up to about 10,000 counts/sec. At higher count rates the response is nonlinear but still calibrated (see Figure 15). As the count rate rises, it becomes necessary to take into account the nonlinear response as well as the increased uncertainty associated with the nonlinear response. Thus, α-Eridanus is so bright that all three photometers have signals in the nonlinear response region; MSP-11 with either filter 3 or filter 4 has the smallest response to α-Eridanus and therefore offers the most precise measurements of this star. Fortunately, we did obtain data through filter 4 of MSP-11 during the 363.3 second sighting. Significant response was seen on pixels 82, 71, 81, 83 and 72. Corrections must be made for background contribution (-3.2 percent), dark count (-0.3 percent), signal lost as the image traversed the gap between pixels (+10 percent), nonlinear correction (+14.8 percent), and atmospheric transmission (+27.5 percent). The corrected mean spectral irradiance is 1632 photons/(cm^2 sec Å) with an uncertainty of 15 percent. This is 3.7 percent lower than that expected from the data of Brune et al.[17] This excellent agreement verifies the accuracy of the calibration. Our observed stellar magnitude for α-Eridanus is 1.7 at 1540 Å. Digicon frames of observations near 36' sec are shown in Figure 51.

Observations for the other stars will be analyzed in the future to obtain stellar magnitudes and possibly to reduce remaining uncertainties in the vehicle attitude reconstruction.
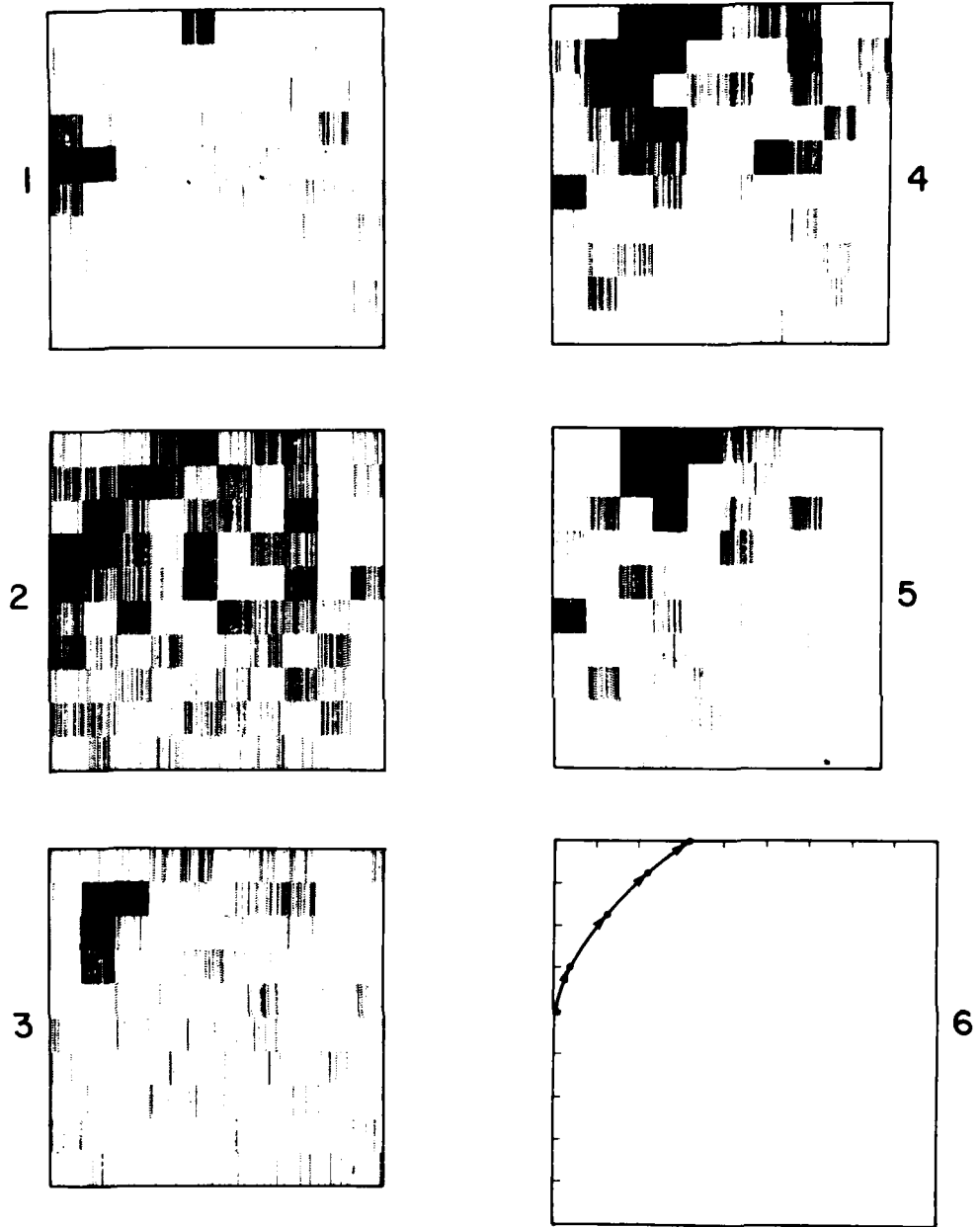
Figure 51.   Stellar Observation by MSP-11, Filter 4.   Dark areas in squares 1-5
show the apparent position of o-ERI in the field of view.   Square 6 shows points rep-
resenting the centroid of the data in squares 1-5.   Mission times corresponding to
the squares 1-5 are 363.2, 363.3, 363.4, 363.5, and 363.6

References

1. Huffman, R.E., LeBlanc, F.J., Larrabee, J.C., and Paulsen, D.E. (1979) Satellite Atmospheric Radiance Measurements in the Vacuum Ultraviolet, AFGL-TR-79-0151.

2. Huffman, R.E., LeBlanc, F.J., Larrabee, J.C., and Paulsen, D.E. (1979) Vacuum ultraviolet backgrounds from space, Society of Photo-Optical Instrumentation Engineers, Proceedings, Vol. 197.

3. Russak, S.L., Flemming, J.C., Huffman, R.E., Paulsen, D.E., and Larabee, J.C. (1979) Development of Proximity and Electrostatically Focused Digicons for UV Measurements from Sounding Rockets, Air Force Geophysics Laboratory, Technical Report, AFGL-TR-79-0006.

4. Huffman, R.E., LeBlanc, F.J., Larrabee, J.C., and Paulsen, D.E. (1979) Satellite ultraviolet airglow backgrounds, Trans. American Geophysical Union, 60:901.

5. Huffman, R.E., LeBlanc, F.J., Larrabee, J.C., and Paulsen, D.E. (1980) Satellite vacuum ultraviolet airglow and auroral observations, J. Geophys. Res. 85:2201-2215.

6. Opal, C., and Carruthers, G. (1979) Naval Research Laboratory, Personal communication.

7. The initial analysis of the attitude control system records and determination of pointing direction was made by AFGL (SU) and Boston College. Figures 18 and 19 have been adjusted based on the additional observations mentioned in the text.

8. Meier, R.R., and Mange, P. (1970) Geocoronal hydrogen: An analysis of the Lyman alpha airglow observed from Ogo-4, Planet. Space Sci. 18:803.

9. Meier, R.R., and Mange, P. (1973) Spatial and temporal variations of the Lyman alpha airglow and related atomic hydrogen distributions, Planet. Space Sci. 21:309-327.

10. Meier, R.R. (1979) Personal communication.

11. Hinteregger, H. (1979) Personal communication.

12. Packer, D.M. (1961) Altitudes of the night airglow radiations, Ann. Geophys. 17:67.

13. Reed, E.I. (1968) A night measurement of mesospheric ozone by observations of ultraviolet airglow, J. Geophys. Res. 73:2951.

14. Reed, E.I., and Chandra, S. (1975) The global characteristics of the atmospheric emissions in the lower thermosphere and their aeronomic implications, J. Geophys. Res. 80:3053-3062.

15. Becvar, A. (1964) Atlas of the Heavens-II, Catalogue 1950.0, Sky Publishing Corp., Cambridge, Mass.

16. Code, A.D., and Meade, M.R. (1976) Ultraviolet Photometry from the Orbiting Astronomical Observatory, An Atlas of Ultraviolet Stellar Spectra, Wisconsin Astrophysics Reports, No. 30.

17. Brune, W.H., Mount, G.H., and Feldman, P.D. (1979) Vacuum ultraviolet spectrophotometry and effective temperatures of hot stars, Ap. J. 227:884.

18. Henry, R.C., Weinstein, A., Feldman, P.D., Fastie, W.G., and Moose, H.W. (1975) Low-resolution ultraviolet spectroscopy of several hot stars observed from Apollo 17, Ap. J. 201:613.

DATE
ILMED

-8